TURNER, ASHLEY R., Ph.D. Studies Examining the Anti-Aging Effects of Fullerenes. (2017)
Directed by Dr. Christopher Kepley. 97 pp.

Research on aging has been invigorated by recent findings suggesting certain mutations in various invertebrate models (yeast, worms, and flies) can slow down aging and improve healthspan. Reactive Oxygen Species (ROS) production and manipulation of the nutrient-sensing [mammalian (originally) or mechanistic target of rapamycin] mTOR signaling pathway have all been linked to aging and age-related diseases. Thus, identifying ways to interfere in these pathways may represent a promising avenue to increase longevity and improve healthspan in mammals. Fullerenes are a class of nanomaterials best known for their ability to significantly extend mammalian lifespan and cognitive function as shown in both mice and rats. Thus, the goal of this proposal is to determine possible mechanisms of how fullerenes extend lifespan focusing on mTOR signaling pathways and anti-oxidant capabilities to slow down aging and improve healthspan.

STUDIES EXAMINING THE ANTI-AGING EFFECTS OF FULLERENES

by

Ashley R. Turner

A Dissertation Submitted to
the Faculty of The Graduate School at
The University of North Carolina at Greensboro
in Partial Fulfillment
of the Requirements for the Degree
Doctor of Philosophy

Greensboro
2017

Approved by

_____
Committee Chair

APPROVAL PAGE

This dissertation written by Ashley R. Turner has been approved by the following committee of the Faculty of The Graduate School at The University of North Carolina at Greensboro.

Committee Chair _____
Christopher L. Kepley

Committee Members _____
Amy Adamson

_____
Will Ethan Taylor

_____
Dennis R. LaJeunesse

_____
Anthony Dellinger

3/20/2017
Date of Acceptance by Committee

3/20/2017
Date of Final Oral Examination

TABLE OF CONTENTS

Page

LIST OF TABLES

Page

LIST OF FIGURES

Page

CHAPTER I

INTRODUCTION

Fullerenes have been regarded as a unique approach to alleviate age-associated diseases, due to their high affinity towards free radicals [1-3]. Fullerene's ability to efficiently scavenge free radicals, without being consumed is attributed to its numerous conjugated double bonds and lowest unoccupied molecular orbital (LUMO) [2]. Previous studies have reported the fullerene derivative C_3 (C_{60}-tris malonic acid) acts as a superoxide dismutase mimetic (SOD) [4], polyhydroxylated C_{60} molecules provided neuroprotection in cultured cortical neurons [5], and C_{70}-tetraglycolic acid (TGA) potential as a therapeutic application for asthma and arthritis in mast cells.

Published reports have linked many age-related diseases to the mammalian target of rapamycin (mTOR) pathway that are critical to age-associated diseases and impairment of function can impact healthspan. Our lab has established that fullerene derivatives C_3 , ALM (a liposome encapsulated C_{70} fullerene) and TGA have the potential to alleviate age-related diseases such as asthma, arthritis and atherosclerosis [6-9] as a novel therapeutic to improve the aging body and overall healthspan. The significance of this research is to assess TGA anti-aging effects in an *ex vivo* human skin model, which has sparked our interest in nanomaterials and its impact on biological aging.

CHAPTER II

REVIEW OF LITERATURE

II. 1 Skin and Aging

Aging research has stimulated innovation in developing novel strategies to investigate the natural biological process of aging. A process that has been attributed to reactive oxygen species (ROS) accumulation in a biological system that was proposed by Denham Harman in 1956 [10], which led to his establishment of the mitochondrial free radical theory of aging [11]. The free radical theory of aging states that cells age due to the accumulation of free radicals over time [10]. Therefore, accumulation of free radicals result in degradation of a biological system, but the contradictory nature of this theory is also in question. For example, ROS production extending lifespan in *S. cerevisiae* by Mrg19 depletion [12]; exercise-induced ROS production inducing antioxidants, DNA repair and protein degrading enzymes and resulting in decreases in oxidative stress-related diseases and retardation of the aging process [13]; and reported increased defense mechanisms prolong lifespan [14, 15].

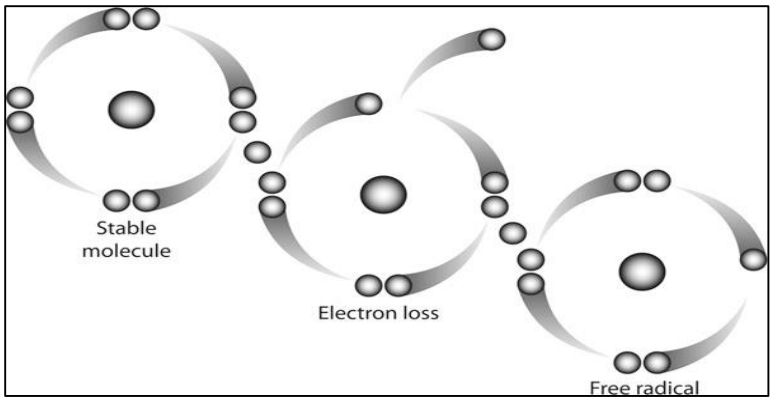

Figure 1. Illustration showing the oxygen molecule and generation of free radicals.
Source: http://www.clevelandclinic.org/reproductiveresearchcenter

If the free radical theory of aging can be both beneficial and detrimental, at this juncture, skin the largest organ in the body, constantly exposed to both intrinsic and extrinsic insults can be classified as a large producer of free radicals and optimal model for aging research. Intrinsic aging is defined as physiological changes (genetics, hormone imbalance, or metabolic reactions) that are uncontrollable and extrinsic aging, to some extent, can be categorized as sun and toxin exposure, diet, pollutions and overall lifestyle choices [16, 17].

In its entirety, the skin is comprised of three distinctive layers: epidermis, hypodermis, and dermis. Here we are focusing on two layers: epidermis and dermis. The epidermis is the outermost layer providing the most protection against UV exposure (*stratum corneum)*, provides mechanical resistance, and immune surveillance [18]. Keratinocytes form the outermost barrier of the skin and react against insults by mediating pro-inflammatory mediators to elicit an immune response. Langerhans are antigen presenting immune cells (dendritic cells), originating from skin localized Ly-6C

monocyte precursors that induce immune response or tolerance; induction of hypersensitivity, and pathogenesis of chronic inflammatory skin disorders [19-21]. Melanocytes function primarily as photoprotection against DNA damage through melanin production; cross-talk between different signaling pathways to maintain skin homeostasis and actively secretes immunological molecules (i.e. IL-10, IL-1α, TNF-α, TGF-β, and nitric oxide) [22]. Merkel cells are associated as a mechno-receptor and paracrine secretion in fetal development and adult homeostasis [23-25].

Directly below the epidermis is the dermis, providing a scaffold for strength and support. While the dermis is a thick layer of elastic and fibrous tissue, it also contains nerve endings, to aid in stress and strain detection. This layer gives elasticity to the integument to resist wrinkling, sagging, and distortion. Fibroblasts are the dominant cell type producing collagen, elastin, glycosaminoglycans, and various proteins in the dermal extracellular space [26]. Fibroblasts have been extensively studied in aging research ranging from organization of the cytoskeleton structure and senescent cells inability to replicate in humans [27]; improved functional and survival ability in mild heat shock treatment *in vitro* [28]; protection by mitochondria targeted antioxidants from endogenous oxidative damage in friedrich ataxia fibroblasts [29]; as well as safety evaluation studies using fullerenes for skin irritation assessment in cosmetic applications [30].

Macrophages play a role in innate immunity, in most tissues, their phagocytic properties are associated with initiating inflammatory response that recruits neutrophils and natural killer cells, regulate maturation, differentiation, and migration of dendritic

cells. The impact of macrophages on innate immunity and aging can be used in identifying endogenous and exogenous "danger" signals emitted from damaged tissues [31, 32]. Macrophages have been used as an *in vitro* model for inflammation and nanomaterial research. For example, exposure to fullerenes induced apoptosis by changing mitochondrial membrane potential and decreasing cell viability [33]; and macrophages/Kupffer cells treated with dihydroquercin suppressed concanavalin A activity in a hepatitis mouse model enhancing heme-oxygenase-1 and MAPK/Nrf2 antioxidant signaling [34]. C_{60} treatment have been shown to modify Th2 to Th1 cytokine production and repair skin barrier function in a mice model of atopic dermatitis [35].

Nanoparticles have been used as vehicles for drug delivery for enhanced bioavailability and skin penetration for deposition of biologically active ingredients [36, 37] and control over compound release to improve efficacy in many skin formulations [37, 38]. For example, alginate, a low cost and biodegradable polymer is ideal for encapsulating antimicrobial plant extract for skin applications [39]. Trans-resveratrol loaded solid lipid nanoparticles penetrated the skin up to 45% after 24 hours, resulting in more tyrosinase inhibition over kojic acid and revealed non- toxic effects in keratinocytes [40], Efficacy of low dose nanoparticles on aging skin preserved spindle shape elongation, characteristics of young fibroblasts as seen using electron microscopy [41]. Efficacy and safety studies are common practices used to create safety profiles surrounding short and long term effects of nanoparticles to determine risk assessment of chemicals, toxins, and nanomaterials through skin absorption [42].

II. 2 Fullerenes as Antioxidants

Carbon based nanoparticles, fullerenes are carbon allotropes identified as ROS scavengers and nano-antioxidants for their potent antioxidant abilities in vitro. Water soluble derivative fullerenes have been designed as effective antioxidants in biological systems to reduce free radical damage to biomolecules. Several fullerene derivatives have been identified as neuroprotective [43], therapeutic treatments against allergic diseases [44], inhibitors of inflammatory arthritis [7] and gene and drug delivery carriers [45, 46]. This notion has been investigated extensively with C_{60} fullerenes, based on their lowest unoccupied molecular orbit (LUMO) and ability to accept up to six electrons has made them suitable electron acceptors [47]. In addition to their knack to react with numerous free radicals without being consumed [2]. These same predictions were made for C_{70} with their spherical shape and potential to counteract the formation of superoxide anion, while a 100% efficiently is sensitized by C_{60}, C_{70} sensitizes only ~81%, in the presence of molecular oxygen [48].

The increased focus on nanomaterials and human health has become an important research element for understanding cellular and tissue influences. Reports on fullerenes have incurred favorable and unfavorable support with regard to the usefulness and therapeutic applications of functionalized fullerenes. Many rely on synthesis methods and chemicals used to produce these functionalized nanomaterials result in assessment of cellular effects due to the biological activity of fullerenes. Acid-treated single walled carbon nanotubes (SWCNTs) and multi-walled carbon nanotubes (MWCNTs) down-regulated adhesion related genes and perturbing physiological functions of actin filaments

of NIH 3T3 cells and human dermal fibroblasts [49]. Hone and colleagues reported C_{70}-medium dispersion induced intracellular ROS levels, however, pre-treatment with antioxidants prevented intracellular oxidative stress in human keratinocytes [50], supporting the notion of a synergistic effect between C_{70} and antioxidants.

Interaction of C_{60} or C_{70} fullerenes with organic solvents can contribute to ROS generation in activated macrophages, as indicated through proinflammatory cytokines. Modulation of pro-inflammatory cytokines, tumor necrosis factor- alpha (TNF-α) was potentiated upon exposure to tetrahydrofyran(THF/nC_{60}/C_{70}) fullerenes causing increased apoptosis/necrosis, however, polyhydroxylated (C_{60}/C_{70} (OH)n) fullerenes reduced TNF-α expression and mitochondrial depolarization. The dichotomy of these fullerenes provides the basis of their use in TNF-α based cancer therapy or deterrence against uncontrolled tissue damage [51]. The unique chemical and physical properties of fullerenes can contribute to beneficial or adverse effects in biological systems, due to their exploitation using innumerable side chain configurations [52, 53].

Nanotechnology's limitless possibilities have introduced compelling candidates, but as humans are the end users for most, if not all applications, these innovations can be challenging to the dermal immune system. To better understand these challenges, well designed studies evaluating innate immunity and ROS derived organelles facilitate closing the knowledge gap supporting longevity and health span research.

Innate immune cells, such as mast cells have been used as proinflammatory mediators in response to immunological and physico-chemical impetuses [7] [54, 55]. Water-soluble fullerenes, dubbed as "radical sponges" utilize electrochemical properties to react with

tissue damaging superoxide ($O_2^{\bullet-}$) and hydroxyl ($^{\bullet}OH$) radicals [51, 56]. Fullerenes, reactive oxygen species modulating agents are ideal interference against TNF-α mediated cell and tissue death [51]. Treatment with C_{60} fullerene, C_3 attenuated age associated oxidative stress, improved cognitive function and extended lifespan in mice [57]. In a report by Hwang and Mauzerall, fullerenes electron-transfer capabilities have made them ideal to mediate transmembrane electron transport across lipid bilayer membranes [58].

Research has taken into consideration fullerene toxicity, adsorption, distribution, metabolism and elimination based on functionalization of moieties for various sized fullerenes. Fullerene derivatives have increased biological application compared to underivatized fullerenes due to their insolubility and potential for aggregation [59]. Exploitation of their small size, large surface area, and affinity to react with numerous superoxides without being destroyed has been advantageous as an antioxidant [2]. C_{70} fullerenes are composed of 70 carbon atoms with a spherical shape made of 25 hexagons and 12 pentagons, its antioxidant property has contributed several double bonds and low lying unoccupied molecular orbit allowing up to six electrons to be consumed [60].

Efficacy of fullerenes and its antioxidant properties are not well understood and an in-depth investigation of mechanisms driving free radical sequestering, in complex biological systems are necessary for improvements in human health.

II. 3 Mechanisms of Fullerenes

Future improvements of lifespan and healthspan could be supported through nanoparticle-based immunostimulatory moieties activating in safe and efficacious combinations with stress response pathway systems. Ideally, using nanotechnology to

advance aging research could aid in modulating ROS production while maintaining feasibility and safety to improving overall human health in biomedical applications. Studying molecular mechanisms underlying fullerenes and mTOR signaling pathways can potentially affect aging by means of altering dermal structure and function. Interactions have been investigated through the use of whole transcriptome methodologies for gene expression modulation after treatment with functionalized fullerenes along the mTOR pathway [61]. Fullerenes provide a promising opportunity for novel therapies as inhibitors in cancer therapy [62, 63] , allergic diseases [44], and arthritis [7].

Our lab has reported possibility for C_{70}-I (*myo*-inositol) functionalized fullerenes as an alternative therapy for steroid resistance asthmatics via inhibition of inflammatory mediators in mast cells. This study reinforced the effects fullerenes have on signaling pathways and modulating immune responses instigated by conventional treatments [64] and the emergence of fullerenes yielding results promising for current and future prospects to ease deleterious side effects of current treatments.

Mechanistic target of rapamycin is a serine/threonine kinase belonging to a family of phosphatidylinositol 3' kinase related kinase (PIKK), a signaling pathway regulating cellular growth, proliferation, survival, and motility, as well as protein synthesis and transcription. The activation of mTOR by PI3K, an upstream regulatory, activating AKT via phosphorylation [61]. Originally discovered through a study using rapamycin, an immunosuppressant and anti-tumor drug, its effect on inhibiting mTOR signaling pathway has been associated in dysregulation of human diseases, such as cancer,

diabetes, synaptic plasticity, memory, learning, and aging [65-67]. The mTOR pathway consists of two complexes: mTOR Complex 1 (mTORC1) known to control autophagy, G1 cell cycle progression, and protein synthesis; and mTOR Complex 2 (mTORC2) is involved in regulating cytoskeletal structure through f-actin polymerization [68-70].

Both mTORC1 and mTORC2 contain components of Deptor (DEP-domain containing mTOR-interacting protein) which inhibits kinase activity [71]; Tel 2 (telomere maintenance 2) and Tti1 (TELO2-interacting protein 1) form a complex to stabilize PIKK proteins and assembly of mTOR complex to maintain activities [72]; while mLST8 (mammalian lethal with sec-13), also known as GβL, function is unclear in mTORC1, but maintains kinase activity in mTORC2 [66]. The protein Raptor (regulatory associated protein of mTOR) has a positive role on mTOR activity and is thought to act as a scaffold, binding multiple contact points and phosphorylation of downstream components (SGK1 and 4E-BP) to mTOR[67], as evidenced by knockdown studies using RNAi in mammalian cells [73]. PRAS40 (proline-rich AKT substrate 40 kDa) an interacting partner with raptor, negatively regulating mTORC1 kinase activity. This association is attenuated by insulin or amino acids, bringing about dissociation of PRAS40 and mTORC1, due to phosphorylation [74] at protein components of mTORC1.

The other functional complex mTORC2, consists of similar proteins (DEPTOR, TEL2, Tti1 and mLST8), containing Rictor, a protein component essential for mTORC2 activity. A study conducted by Lammin et al [75] provided evidence that deletion of Rictor decreased lifespan in male mice, not females. The protein mSIN1 (mammalian stress-activated protein kinase interaction protein 1) stabilizes the mTORC2 complex

through specificity with SGK-1 (serum glucocorticoid-induced protein kinase 1), PKB (protein kinase B/Akt), and PKC (protein kinase C), while Protor-1/PRR5 (Proline Rich Protein 5) is not required for activity [76] and does not bind nor sensitive to FKBP12-rapamycin complex[77, 78]. Although, little is known about mTORC2 role in aging and age-related pathologies; it is known that phosphorylation of the hydrophobic regulatory region of PKB, SGK, and a few PKCs can promote cell survival. Furthermore, cytoskeleton and cell motility is regulated by small Rho GTPases, and Paxillin within mTORC2 complex [79]. Activation of oncogenes PI3K, PKB, and Ras or inhibition of PTEN or p53 can dysregulate cellular metabolism and survival, therefore leading to age related pathologies.

The FKBP12 rapamycin complex is necessary for binding to mTOR, through the FKBP12 rapamycin binding domain (FRB). This ternary protein containing FKBP12 is a rapamycin-induced complex required for cell cycle progression and growth mediated by rapamycin. Any mutation (point) can lead to FKBP12 rapamycin binding domain resistance to mTOR, particularly by modification of the mTORC1 structure [66, 68].

Cellular processes regulating proliferation, growth, and metabolism can be traced to mTOR signaling pathway controlled via mTORC1 or mTORC2. The most well studied and understood complex, mTORC1 can be activated through stress, nutrients, oxygen levels, and growth factors [80]. Sensing both intracellular and extracellular stimuli directly instigates downstream proteins: S6K1 (S6 kinase), 4E-BP1 (eukaryotic translation initiation factor 4E-binding protein 1), and SREBP (sterol regulatory element-binding protein) and autophagy components encouraging protein synthesis, lysosome

biogenesis, and deterring autophagy [81]. Growth signals incorporated through mTOR complex 1 sensing energy and nutrient levels encourage proliferation upon promising conditions and autophagy upon traumatic conditions [82].

Tissue damage and repair has be examined through S6K1, a downstream regulator, once activated promotes axon regeneration in a mouse optic nerve crush CNS injury model by deleting PTEN (phosphatase and tensin homologue) and TSC1 (tuberous sclerosis 1), but not inhibition of 4E-BP [83]. The activation or deactivation of mTORC1 upon cell or tissue damage invokes molecular signals or biomarkers to initiate adequate responses. For example, enhanced stress resistance and longevity genes were discovered in nematode model through inhibition of mTORC1 signaling by regulating SKN-1/Nrf2 stress transcriptional factor, which is required along with rapamycin [84]. Multiple mechanisms are involved in mTOR signaling and mitochondrial function in yeast models, demonstrated inhibition on mTORC1 increased chronological lifespan by shifting mitochondrial respiration [14].

Understanding the inner workings of mTORC2 is not well understood or documented as mTORC1. Mechanisms regarding how stimuli is detected has been addressed in yeast and eukaryotes seemed unresponsive to rapamycin (short term treatment) and function upstream of Rho GTPases regulating the actin cytoskeleton [85]. Once activated by ribosomes, mTORC2 solicits help through binding of PI3K, however, this mechanism is poorly defined [86]. Several members of AGC (protein kinase A, G and C) family of kinases are governed by mTOR complex 2 including Akt, SGK 1(serum- and glucocorticoid-induced protein kinase 1) and PKC-α [87].

Phosphorylation of AKT at its hydrophobic motif (Serine 473) is required for maximal activation of metabolism, cell survival, and apoptosis [88]. Lamming and colleagues provided some insight on the role of mTORC2 in three different mouse models of RICTOR depletion: heterozygous for RICTOR, RICTOR deleted in the liver, and RICTOR induced deletion throughout the mouse model. Chronic long term treatment of rapamycin does effect mTORC1, as well as mTORC2 *in vivo,* however longevity was gender specific, with females outliving their male counterparts [89].

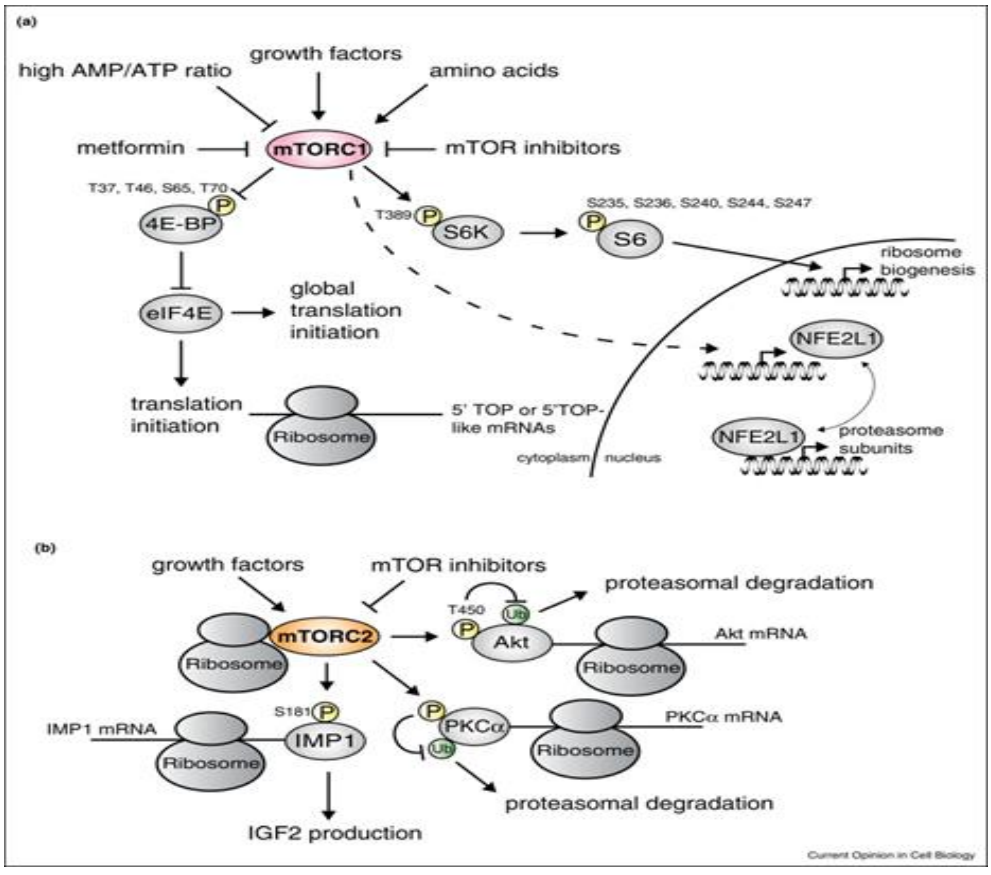

Figure 2. Mammalian Target of Rapamycin (mTOR) controls protein synthesis.[90]

Interestingly, induction of cytoprotective measures suggests a link between mTOR and antioxidant activity, to some degree in some organisms to control a spectrum of autoimmune diseases [91, 92], lifespan [35], and mental cognitive abilities [93] [94]. Pharmacological blockage of mTOR and personalization aimed toward lifespan show promise, but not without some adverse events, nonetheless, preventive measures against metabolic and neurodegenerative abnormalities provide ideal solutions in the form of mTOR inhibitors.

CHAPTER III

EFFICACY OF NANOPARTICLES IN AN EX VIVO HUMAN SKIN MODEL OF AGING

III. 1 Introduction

The skin is the largest and most exposed organ of the body reacts to both natural and man-made compounds, making it an ideal model to discern nanoparticle penetration. Fullerenes and other substances ability to traverse the skin usually occurs at the stratum corneum (Figure 3), outermost layer of the epidermis with a thickness of about 10-40μm [95, 96]; this is the rate limiting barrier for absorption of topical formulations [42, 97]. The route of penetration may occur through hair follicles, sweat ducts, intercellular and intracellular corneocyte openings [98, 99]. A thorough understanding of nanoparticles penetration process, accumulation in the dermis, and permeability of the stratum corneum is not complete and requires more dermal exposure studies to provide a realistic representation surrounding skin absorption and nanoparticles [100, 101].

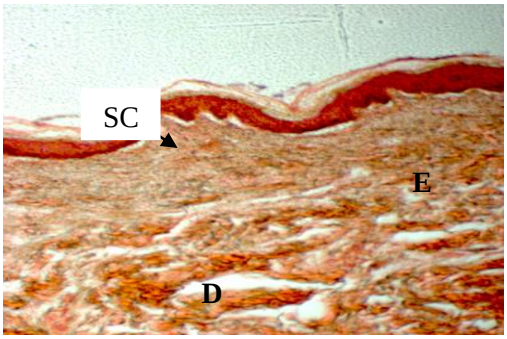

Figure 3. Hematoxylin and Eosin (H&E) staining representing the three layers of human skin. Stratum Corneum (SC), Epidermis (E), and Dermis (D).

Advancement in nanotechnology have made modifying nanoparticles into lipophilic or hydrophilic properties to capitalize on its ability to alter skin morphology. It has been well documented that lipophilic molecules less than 600 Daltons (Da) can penetrate the skin passively [102], while some have placed maximum size at 400 Da for intact skin [103]. Certain areas of the skin allow for nanoparticle penetration, due to the lipophilic (stratum corneum) and hydrophilic (epidermis) nature of skin [104]. while, others argue due to fullerenes molecular weight (720 Da) prevents skin penetration [105]. Nanoparticle formulations efficacy on skin can be based on alteration of microscopic structures which can be examined by quantitative and qualitative measurements. Souto et al [106] reported increased permeation of C_{60}-poly(vinylpyrrolidone) (PVP) upon UVA irradiation, indicating human skin being less permeable than porcine skin by means of skin diffusion techniques.

We investigated three nanoformulations (NF) and found remarkable results in their ability to provide protection and alter skin architecture. Each nanoformulation is comprised of different functionalized, water soluble fullerenes and efficacy is evaluated between different formulations and untreated controls. We used aged human skin as an *ex vivo* model to scientifically document the effects of each nanoformulation alongside control, on the basis of skin morphology and histological assessment.

III. 2 Methods

III. 2 .1 Fullerene Preparation

All fullerene derivatives were obtained from Luna Innovations, Danville, VA. Each compound (described previously) [16, 107] was characterized using HPLC, NMR,

and MALDI mass spectroscopy. After filtering through 0.22 uM sized membrane filters, water solubility was assessed visually using light microscopy and particle sizes were analyzed by dynamic light scattering.

III. 2 .2 Ex vivo Skin Model

Human skin was obtained with informed consent from a 35-49 year old females, undergoing abdominal or breast reduction from the Cooperative Human Tissue Network. All studies were approved by the Human Studies Institutional Review Board. Samples had excess fat removed and was placed in RPMI 1640 media (Life Technologies, Carlsbad, CA) supplemented with streptavidin and L-glutamine, 10% fetal bovine serum, HEPES, and amphotercin B for ~ 1.5 hours. Afterwards, skin was cut into pieces and placed in a 24-well plate with culture medium and incubated at 37°C in 5% CO_2. Samples were treated with C_3 (C_{60}-tris-malonyl acid), TGA (C_{70}-tetraglycolate), DMAE (C_{60}-Dimethylethanolamine) or untreated (control) for two weeks.

III. 2 .3 Scanning Electron Microscopy

Documenting the effects of substances used on skin have been useful to visualize alterations in skin surfaces for protein deposits on hair shafts and skin roughness [108]. Thus, we used scanning electron microscopy (SEM) on human skin tissue that was treated with C_3, DMAE and TGA at 1 μg/ml over a two week period. Skin was rinsed with 0.1M phosphate buffered saline for 10 minutes and immersed in glutaraldehyde for 24 hours at room temperature. Skin swatches were washed again to remove excess fixation solution. Afterwards, swatches were dehydrated with an increasing gradient of acetone at room temperature. Hexamethylsilane (HMDS) was used to remove excess

liquid from the skin sample. Samples were attached to electron microscopy stubs using carbon tape and sputter coated with ~10 nm of gold palladium on a Denton Vacuum Inc. Desk II Sputter Coater (Denton Vacuum LLC, Moorestown, NJ, USA). Images were captured using a Carl Zeiss Auriga SEM-FIB at magnifications of 47X, 250X and 615X.

III. 2 .4 Histology

Tissues were placed in 70% ethanol and shipped to IHC world (Ellicott City, MD, USA) for cutting and staining with Hematoxylin and eosin (H&E) and Masson-Trichrome, a three color staining to determine cellular components and epidermal-dermis integrity. Histological procedure was performed in accordance with manufacturer's instructions. Specimens were visualized using a Zeiss Axio light microscope (Carl Zeiss AG, Peabody, MA, USA) for histopathological examination. Histometric analysis was assessed by measuring 150 micrometer width across a 20X H&E image. Six vertical lines were drawn from top of epidermis (minus stratum corneum) to stratum basale to transverse across the 150 micrometer width line to collect measurements using Zeiss Axio light microscope.

III. 2 .5 Statistical Analysis

The data used for histological analysis was analyzed using GraphPad Prism 5.0 (San Diego, CA) and presented as mean ± SD. A one-way analysis of variance followed by Tukey post test, where $p<0.01$ was considered significant and highly significant as $P<0.001$.

III. 3 Results

We used an ex vivo human skin model to assess the skin surface changes induced by three nanoformulations. Control samples (Figure 4A) exhibited some flaking and cracking on the stratum corneum, indicative of unhealthy, damaged skin. Skin samples treated with the DMAE, C_3, and TGA (Figure 4B, C, and D) displayed minor cracking, but less severe compared to untreated naturally aged human skin sample. SEM images of skin specimens demonstrated our nanoformulations was more effective at preserving the stratum corneum than untreated human skin samples.

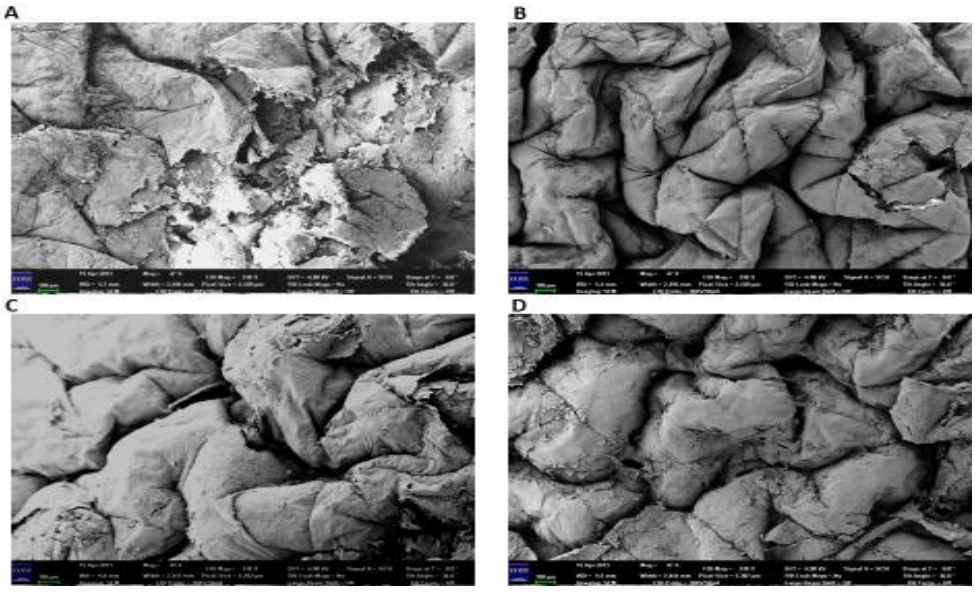

Figure 4. Nanoformulation creams prevent dermatological destruction associated with aging. Human skin tissue was processed using an ex vivo skin model were treated with various NF (1 μg/ml) over a two week period. Scanning electron microscopy (47X) was used to image samples. Skin pretreatment with A) Control, B) DMAE, C) C_3, D) TGA resulted in less flaking of the stratum corneum when compared to control untreated skin.

Skin absorption/penetration was remarkable with the three nanoformulations as determined by the quality of the stratum cornuem. Scanning electron microscopy images

from human skin of control, C_3, DMAE and TGA groups are presented in Figure 5. In Figure 5A, the image depicts severe damage of untreated skin showing desquamation or skin peeling of the tissue at the outermost layer. Moderate flaking for DMAE (Figure 5B), C_3 (Figure 5C), and TGA (Figure 5D) at higher magnification (250X). Slight peeling on the surface (Figure 5C) revealing pores underneath the stratum corneum can be classified as marginal drying of the skin.

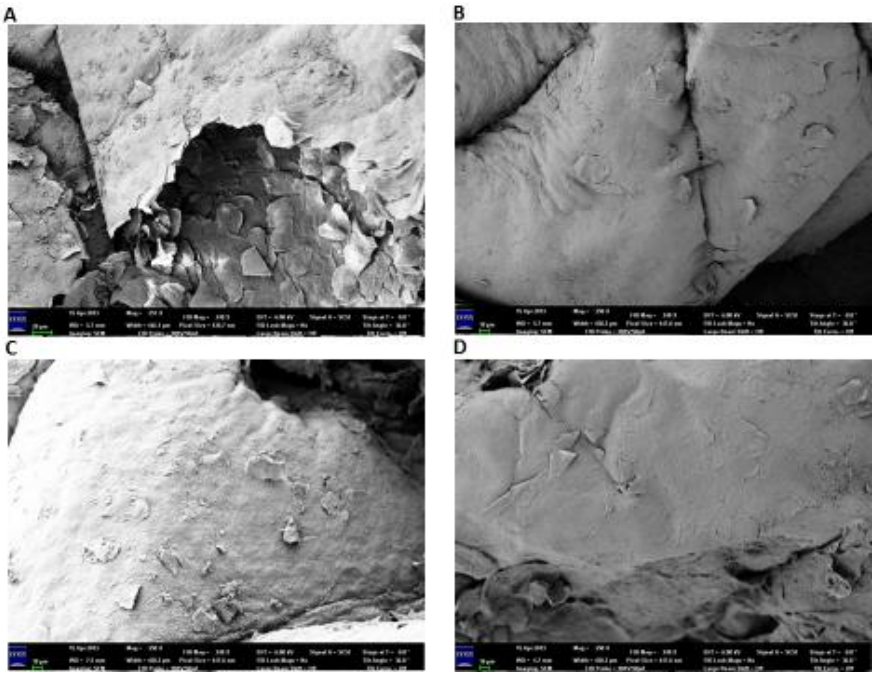

Figure 5. Skin absorption of nanoformulations prevents desquamation. Human skin tissue was processed using an ex vivo skin model were treated with various NF (1 μg/ml) over a two week period. Scanning electron microscopy (250X) was used to image samples. Skin pretreatment with A) Control, B) DMAE, C) C_3, D) TGA resulted in smoother appearance of the stratum corneum when compared to untreated skin.

Upon closer SEM examination (615X) definite improvement in skin quality proved DMAE and TGA (Figures 6B and 5D) delivered a smoother surface area in comparison to control (Figure 6A). In Figure 6C, C_3 did appear to have a slight reduction

of desquamation in the outermost layer after two weeks of treatment, confirming some beneficial effect over control group but not at levels of DMAE and TGA. Prominent scaling or sheeting seen in Figure 5A (control) measured by the number of raised layers on the stratun corneum, indicated quantitatively the efficacy of the nanoformulations. Higher magnification for control group (Figure 6A) produced many papule-like structures on the epidermis. Treatment groups DMAE and TGA (Figure 6B and 6D) did not present similar structures, but C_3 (Figure 6C) exhibited some characteristics as control group.

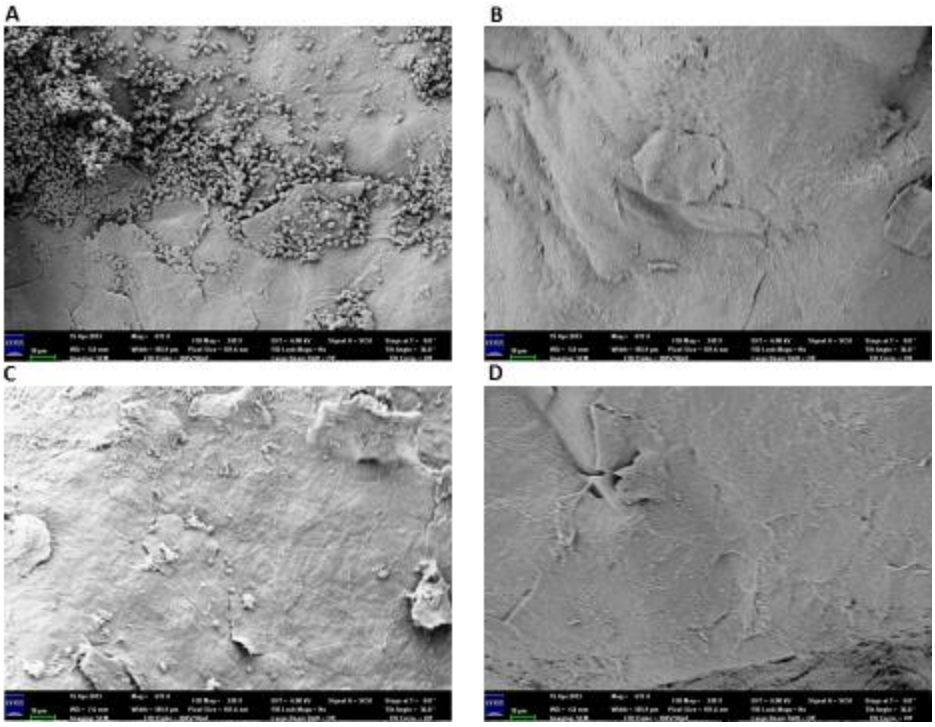

Figure 6. Nanoformulations prevented papular formation. Human skin tissue was treated with various NF (1 μg/ml) over a two week period. Scanning electron microscopy (615X) was used to image samples.Skin pretreatment with B) DMAE and D) TGA resulted in smoother appearance no papular formation on the stratum corneum when compared to A) untreated and C) C_3.

To further prove efficacy in an *ex vivo* human skin model, evaluation of three nanoformulations was assessed by hematoxylin and eosin (H&E) staining to determine possible tissue pathologies. The results obtained are presented in Figure 7, which shows a transverse section of all groups for characterization of layers and structures of skin organization. Samples treated with nanoformulations (Figures 7B-D) verified SEM images (Figures 4-6) and little to no morphological changes in stratum corneum layers were detected in comparison to control (Figure 7A). Histologic analysis revealed tact stratum corneum, epidermis, and dermis of DMAE and TGA (Figure 7B and 7D) over untreated group (Figure 7A) and C_3 (Figure 7C).

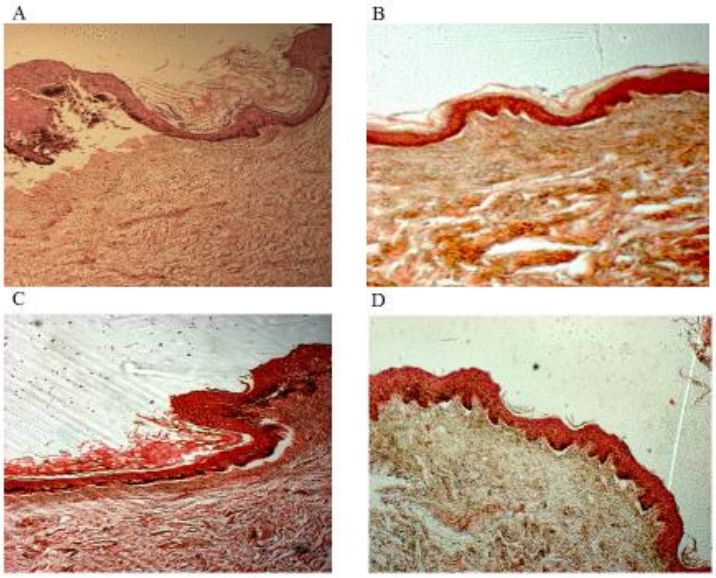

Figure 7. Nanoformulations prevent age-related epidermal detachment. Skin samples treated with and without fullerenes (1 μg/ml) were placed in 4% paraformaldehyde, mounted, and stained with Hematoxylin and Eosin (H&E, 10X). The NF prevented the detachment of the epidermal layer compared to non-treated sections. Groups represented as A) Control, B) DMAE, C) C_3, and D) TGA.

Microscopically, the human skin model stained with Masson Trichrome revealed connective tissue (dark blue), nuclei (red/purple), and cytoplasm (red/pink) as represented in Figure 8. Epidermis and dermis region appeared to be detached from the basement membrane in the untreated group (Figure 8A) in comparison to treatment groups (Figure 8B-D). In Figure 8B, DMAE produced an intact stratum corneum, epidermis, and dermis sections, as well as healthy collagen bundles and epithelial cells. On the other hand, C_3 (Figure 8C) showed epidermal-dermis disorganization and separation at the junction. In Figure 8D, TGA caused less epidermal-dermis detachment over control group (Figure 8A).

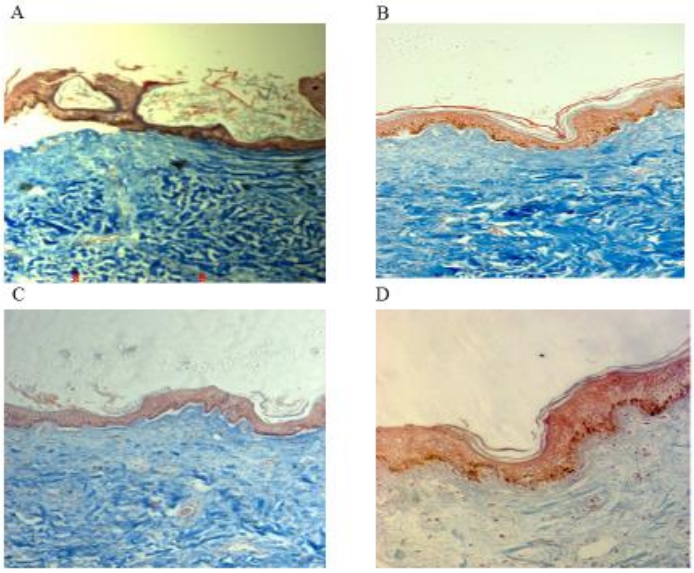

Figure 8. Masson Trichrome staining of skin untreated and treated with nanoformulations. A) Control, B) DMAE, C) C_3, and D) TGA groups treated over a two week period. Skin samples processed, mounted, and stained with Masson's trichrome (10X). Histological images of collagen bundles (dark blue),cytoplasm (red/pink) and nuclei (dark red/purple).

All nanoformulations displayed distinct stratified squamous keratinized epithelial consisting of keratinocytes, melanocytes and corneocytes in the epidermis layer as well as

fibroblasts in the dermis region (Figure 9). The stratum basale presented a more uniform layer of melanocytes and keratinocytes for DMAE (Figure 9B) and fibroblast placement in the dermis using higher magnification (20X) as compared to control and other treatments groups (Figure 9C, and 9D). In comparison with control (Figure 9C), C_3 presented slight detachment of the epidermis-dermis junction but better protection was seen over a two week period in comparison to control. Melanocytes appeared less plentiful at the basement membrane (stratum basale) and pale-nuclei of keratinocytes located in the stratum spinosum are more pronounced over control (Figure 9A and 9C). In Figure 9D, stratum basale is heavily populated with resident melanocytes, while keratinocytes reside in the upper epidermis layer (stratum spinosum); in addition corneocytes (anucleated cells) can be seen in the upper most layer (stratum granulosum) of TGA nanoformulation in comparison to control.

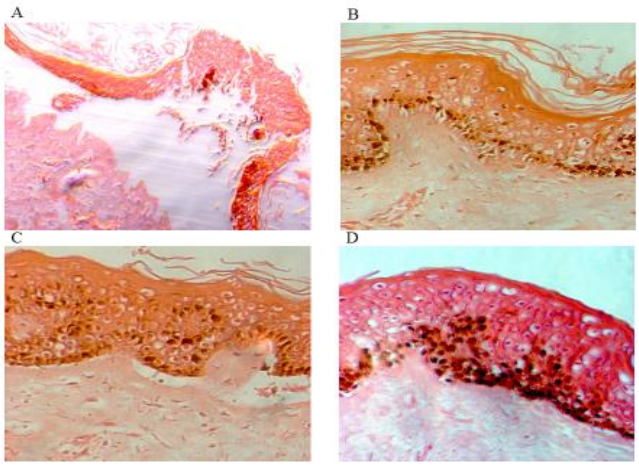

Figure 9. Distinct cell types in the epidermis and dermis layers of skin. Epidermal-dermis junction using Hematoxylin and Eosin (H&E) staining of human skin (20X). Stratified squamous keratinized epithelium and connective tissue of the dermis layer displayed in A) Control, B) DMAE, C) C_3, and D) TGA.

Moreover, a diminishing stratum corneum is apparent in all three nanoformulations with a complete dissolution in the control group (Figure 10). Densely

populated melanocytes and kerationcytes residing in the stratum basale followed by the stratum spinosum layer of DMAE, C_3, and TGA (Figures 10B-10D) in comparison to control group (Figure 10A). In Figures 10B-10D, all nanoformulations produced normal viable cells of the stratum spinosum with well uniform melanocytes and keratinoctyes. However, separation of the epidermal-dermis section is seen in C_3 (Figure 10C) over DMAE and TGA (Figures 10B and 10D) compared to control. Dermal collagen bundles and fibroblast of treatment groups did not show any significant difference to that of control.

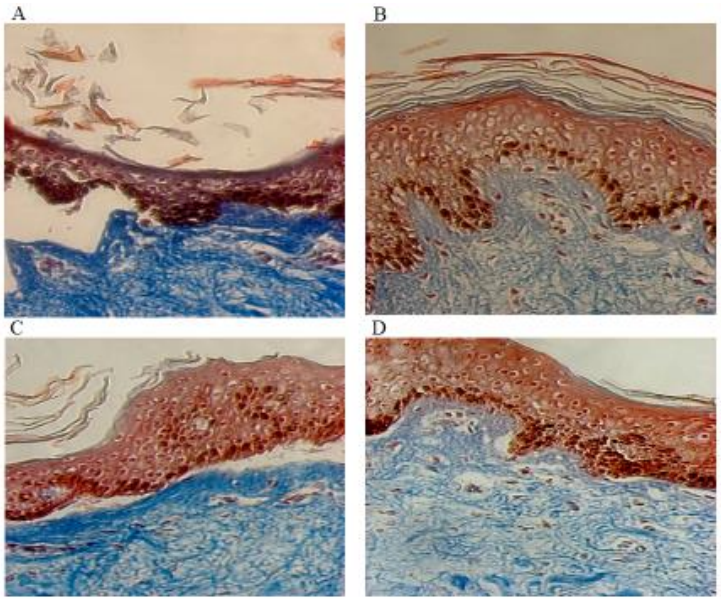

Figure 10. Masson Trichrome staining of epidermal-dermis layers of skin.
After two weeks of treatments, skin samples were stained with Masson Trichrome (20X). Collagen bundles (dark blue), cytoplasm (red-pink) and nuclei (dark/red) can be seen in all groups A) Control, B) DMAE, C) C_3, and D) TGA.

A visual difference was detected in the epidermis region of all groups. Measurements were taken from stratum lucidum (thin clear layer between stratum

corneum and stratum granulosum) to the stratum basale (bottom of epidermis). Epidermal thickness was highly significant ($p<0.001$) for DMAE and TGA while C_3 significantly ($p<0.01$) increased over control (Figure 11).

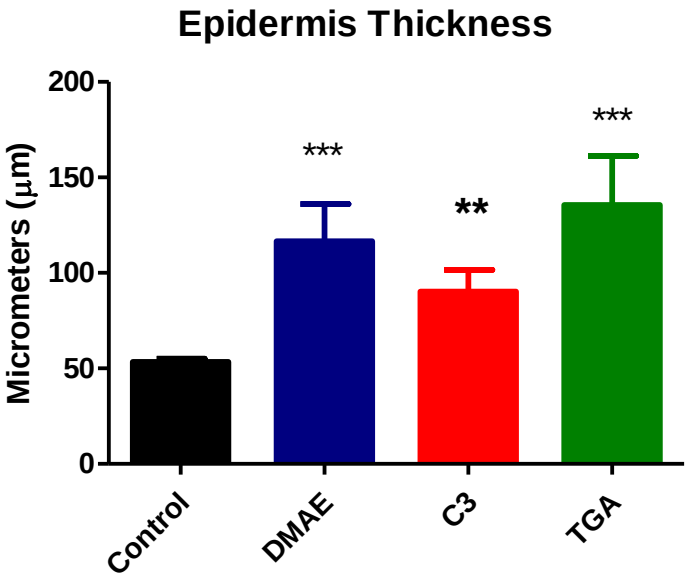

Figure 11. Measurement of epidermal thickness. Epidermal thickness of human skin treated with Control, DMAE, C_3, and TGA nanoformulations over a two week period, without stratum corneum. Significance denoted as **$p<0.01$ and ***$p<0.001$.

III. 4 Conclusions

To examine the intricacy of skin tissue morphology induced by our nanoformulations, histological and scanning electron microscopy techniques provided an understanding of skin penetration/absorption with fullerenes. After two weeks of topical treatment, DMAE and TGA maintained an intact epidermis-dermis junction, whereas C_3 and untreated showed signs of disruption. These finding imply our nanoformulations resulted in some protective modifications of the outermost layer of the skin and no collagen degradation in the dermis region at a 1µg/ml concentration.

Scanning electron microscopy evaluation of three nanoformulations for their ability to topographically alter epidermal skin architecture as shown in Figures 4-6, after two weeks of topical treatment. Microscopy images confirmed treatment groups produced a smoother, supple, and healthier surface area over control group, most notably DMAE and TGA. Grossman[109], investigated the safety and efficacy of DMAE (dimethylaminoethanol) proving acute skin firming effects measuring quantitatively cutaneous tensile strength and improvements ($p<0.05$) in periorbital fine wrinkles, under eye dark circles and neck firmness.

These findings support our histological analysis (Figures 7B, 8B, 9B, and 10B) of fibroblast proliferation in the dermis aiding to increased structural integrity by secreting collagen. Upon microscopic examination, DMAE epidermal thickness and dermal density was increased compared to control (Figures 7-10). The same outcome was seen in using DMAE alone and in combination with an amino acid (AA) compound, once a week for 4 weeks of microinjections in rats [110]. According to Proksch et al., skin hydration is correlated to integrity of the stratum corneum, indicating good functionality of skin mechanism [111].

The effects of C_3 on skin surface roughness was observed by SEM and histology after two weeks of treatment. Skin flaking can be detected (Figure 6C) but not as severe as untreated skin tissue (Figure6A). Similar results were reported using polymeric nanospheres incorporated with water-soluble methylcellulose, for enhanced permeation in human cadaver skin after SEM analysis exhibiting some skin flaking [112]. C_{60} fullerenes are the most studied nanoparticle due to their ability to scavenge free radicals.

What is known about C_3 through Dugan et al, is the ability of C_3 to act as an superoxide dismutase (SOD) mimetic increasing lifespan, reducing free radical production, increased mental plasticity in Morris water maze and diminishing age-related immune system responses [113, 114]. Interestingly, water-soluble functional groups attached to fullerenes reduced cytotoxicity over pristine C_{60} fullerenes[115]. This suggest C_3 provided some protection against skin surface morphology and cellular function.

Microscopic examination of TGA after two weeks of treatment produced an increase in epidermal thickness compared to that of control (Figures 9D, 10D and 11). This is supported through morphological changes associated with an increased number of cells and furrow of the epidermal-dermis junction, indicating proliferating epidermis, leading to skin improvement [116]. As previously reported, TGA inhibited cytokine production of synovial fibroblast and osteoclast production in an *in vivo* efficacy study [7]. This debunks the notion, TGA provokes inflammatory cells leading to increased epidermal thickness. Upon testing the efficacy of TGA, on an aging skin model, it warrants further investigation based on previous research due to its lack of build-up in tissue, therefore limiting toxicity[8].

Skin penetration of nanoparticles can be a common strategy for drug delivery to transverse intact skin, through weakening highly organized epidermal barrier consisting of lipids, stratum corneum, and other epidermal layers [117, 118]. The stratum corneum (15μm thick) acts as a barrier to prevent chemicals and particulates from entering the body, comprised of anucleated cells (corneocytes) entrenched in a uninterrupted intercellular lipid matrix [105]. In Figure 11, a significant difference in epidermal

thickness was discovered with all nanoformulations with DMAE and TGA demonstrating impressive protection over control. Keratinocytes differentiation, proliferation, and cellular death regulates epidermal thickness [119], however, a careful balance must be maintained.

Topical nanoparticles effect on cell morphology and function has come into question surrounding viable epidermis ability to change cellular organization. A study conducted by Leite-Silva et al. noted topical application of zinc oxide nanoparticles on the epidermis did not alter metabolic state or morphology of cells in a skin penetration study [120]. Although, our nanoformulations differ from Leite-Silva, no cellular morphology was detected in this study using topical application in aged human skin. Generally speaking, skin penetration of nanoparticles is size, shape, and charge dependent as well as mechanical flexion [121, 122]. Additional studies to evaluate toxicological effects will need to be conducted to determine safety of these fullerenes in human skin.

CHAPTER IV

TOXICOLOGICAL ASSESMENT OF NANOFORMULATIONS

IV. 1 Introduction

Toxicological evaluations are necessary to understand safety profiles of functionalized fullerenes in biological organisms. Conflicting reports surrounding toxicity and inflammatory potential of fullerenes vary based on size[123] , moieties[124], and concentration [125, 126]. To address toxic effects of fullerenes a series of experiments are needed to estimate genotoxicity, cytotoxicity, dermal and ocular irritations corresponding to nanomaterials and biocompatibility. Most studies have focused on short or acute toxicity of fullerenes [127-130] but information on long-term human and animal studies are scarce and essential for a thorough risk assessment [42].

Functionalized fullerenes are attractive nanoparticles due to their cellular interactions and solubility in biological systems. C_{60} and C_{70} fullerenes uniqueness stems from small size, large surface area, and affinity to react with numerous superoxide anions without being destroyed is an advantage as an antioxidant [2]. Radical scavenging efficiencies of C_{60} and C_{70} fullerenes favor carbon-centered free radicals [131] but toxicity of biological function is dependent of chemical moieties attached to the carbon cage [44]; allowing up to six electrons to be consumed[2].

Characterization of chemical toxicities using in vitro cell culture models are traditional methods used to screen various concentrations of fullerene derivatives.

However, this method, although useful does not fully capture the functionality and structural changes associated with ex vivo models of a particular organ system under oxidative stress. Fullerenes have been branded, potent antioxidants, due to their ability to scavenge free radicals [5, 132], protect mouse myoblast cells from oxidative induced stress [133], and inhibit organophosphate induced acetylcholinesterase toxicities [134] and extend lifespan and rescue age related cognitive impairment in mice [57]. As an emerging topic in research, employing fullerenes as novel treatments for cancer, diabetes, autoimmune disorders, rheumatoid arthritis, atherosclerosis and hypertension and physiological aging can be useful for future therapeutic applications [135, 136].

Literature has presented conflicting claims some demonstrating fullerenes as potent antioxidants in various cell and tissue types [137, 138], while others have disputed this claim [139, 140]. This study is to elucidate functionalized fullerenes mechanism of reactive oxygen species generation or elimination, investigated through toxicological endpoints.

IV. 2 Methods

IV. 2 .1 Fullerene Derivatives

All fullerene derivatives were obtained from Luna Innovations, Danville, VA. Each compound has been described previously [16, 107]. Each was characterized using HPLC, NMR, and MALDI mass spectroscopy. After filtering through 0.22 uM sized membrane filters, water solubility was assessed visually using light microscopy and particle sizes were analyzed by dynamic light scattering.

IV. 2 .2 Human Cell and Tissue Culture

Human skin samples were obtained as noted above (Chapter 3, Methods) and 3T3 fibroblasts (ATCC) were maintained at 37°C in a humidified atmosphere with 5% CO2, in a HEPES (20mM)–buffered RPMI 1640 cell culture medium (Sigma-Aldrich) supplemented with 10% fetal calf serum, 2mM L-glutamine, and 100 IU/ml penicillin and streptomycin (Sigma-Aldrich).

IV. 2 .3 Bacterial Mutagenicity Assay

To detect potential fullerene induced gene mutation, *Salmonella typhimurium* a bacterial reverse mutation assay was used to assess DNA damage. Various concentrations of fullerenes were mixed with 5 μl of *S. typhimurium (TA100*) along with reaction mixture and grown overnight. Sodium azide was a standard mutagen (positive control) and reaction mixture and water (Background) were included in the assay. Aliquots of 200 μl of sample material, positive control, and background were added to a 96 well plate. Plates were covered and sealed in an airtight plastic bag and incubated at 37°C for three to six days. Colorimetric analyses of results were based on the number of yellow wells (mutated) present in each sample material compared to purple wells (non-mutated).

IV. 2 .4 Lactate Dehydrogenase (LDH) Cytotoxicity Assay

To evaluate the release of the enzyme lactate dehydrogenase (LDH) from human skin tissue treated with functionalized fullerenes. Tissues were placed in a 24 well plate and media added at the air-liquid interface, exposing only the top layer of the skin (stratum corneum). Tissue samples were treated with either DMAE, C_3, TGA, or media (control) for two weeks. The release of LDH into tissue culture media was assessed

using a commercially available LDH Cytotoxicity Detection Kit (Clontech, Mountian View, CA) arding to manufacturer instructions. Experimental controls were as followed: Background: tissue culture media and Negative Control: culture media plus tissues. Positive Control: tissue treated with 100µM H_2O_2. Supernatant (100µl) was removed from all groups and plated into a 96-well plate, 100µl LDH assay solution was added to each well. Plates were incubated at room temperature for 30 minutes. Absorbance was measured at 490nm wavelength. Average of absorbance was calculated for each group in triplicate.

IV. 2 .5 Metabolic Activity Assay (MTT)

Metabolic activity of 3T3 cells treated with functionalized fullerenes was measured using the MTT assay (Invitrogen) based on manufacturer's instructions. Trypan blue was used for cell counting and resulted in 96% viability of untreated cells. Cells were plated in a 96 well plate at a density of $1x10^6$ cells/well and treated with media (Control), 50µM H_2O_2. 1µg.ml TGA, or 50µM H_2O_2/1µg.ml TGA (combination). Groups were incubated at 30 minutes, 1 hour, 2 hours, 4 hours, 8 hours, 12 hours, and 24 hours at 37°C in 5% CO_2. After designated incubation timepoints, supernatant was removed and rinsed with phosphate buffer saline. A 10µl of MTT reagent was added to all wells and plates incubated at 37°C for 4 hours. Solution was aspirated from each well and 100µl of dimethyl suphoxide (DMSO), resulting in formazan crystals solubizing in each well. Abosrbance intensity was detected by plate reader (BioTek, Winooski, VT) at 570nm. All experiments were performed in triplicate.

IV. 2 .6 Reactive Oxygen Species (ROS) Measurement

To measure intracellular production of reactive oxygen species, oxidation-sensitive fluoroprobe 2′,7′-dichlorofluorescin diacetate (DCFH-DA) fibroblasts were exposed to functionalized fullerene at preactivation, 0, 30 and 60 minute timepoints. All parameters were expressed in relative fluorescence units and percent increase or decrease in ROS formation compared to control (negative) not treated with H_2O_2 or TGA. Adherent cells was incubated with 100µM carboxy-H_2DCF at preactivation, 0, 30, and 60 minutes. A working solution was made from a stock prep of DCF, using 100mM DCF-DA plus 2.0 ml of loading media (99% basal RPMI 1640 + 1% Fetal Bovine Serum) into microcentrifuge tube. Removal of carboxy-DCF was done by rinsing with PBS and adding 1.0 ml PBS containing fullerenes, hydrogen peroxide, or L-ascorbic acid (Sigma-Aldrich) .to designated test wells. Fluorescence of DCF at pre activation, 0, 30, 60minutes was detected by plate reader (BioTek, Winooski, VT) with excitation and emission wavelength of 485 and 530nm.

IV. 2 .7 Phototoxicity Measurement

Fibroblasts cell were exposed for 30 minutes of light and dark, to measure the effects of ultraviolet (UV) radiation on 3T3 cells. Cells were seeded $0.5x10^6$/cells in a 96 well plate and incubated at 37°C at 6% CO_2. Two plates were used and cells treated with media (Control), 100µM L-ascorbic acid (Negative control), 100µM H_2O_2 (positive control), 0.01µg TGA, and 1.0µM TGA. Plate exposed to lighr was put into UV chamber for 30 minutes, while second plate was light protected using aluminum foil. After 30 minutes, 100µl of supernatant was aliquoted into another 96 well plate. A 10µl sample of

MTT reagent was added to each well, incubated for 2 hours at 37°C in 6% CO2. All plates were run at 590nm absorbance using a plate reader (BioTek, Winooski, VT) measuring colrimetric results. All samples were ran at an n=6 for statistical analysis.

IV. 2 .8 Statistical Analysis

The data used for MTT, LDH, ROS formation, and photoxicity experiments were analyzed using GraphPad Prism 5.0 (San Diego, CA) and presented a mean ± SD. Data was analyzed by one-way ANOVA using Tukey's or Newman-Keuls multiple comparison post hoc test (comparison of more than two groups).

IV. 3 Results

Fullerene treatment did not mutate *Salmonella typhimurium* (TA100) compared to positive control sodium azide, a known DNA mutagen used to assess genetic modification of unknown chemicals. No mutagenic potential was detected for treatment groups at all dose concentrations (1.0, 0.1, and 0.01 µg/ml) treated with either DMAE, C_3, and TGA after observing test samples through Day 6 (Figure 12). Statistical analysis was conducted using two-way ANOVA, Bonferroni post test to compare sodium azide (positive control) to groups over six days.

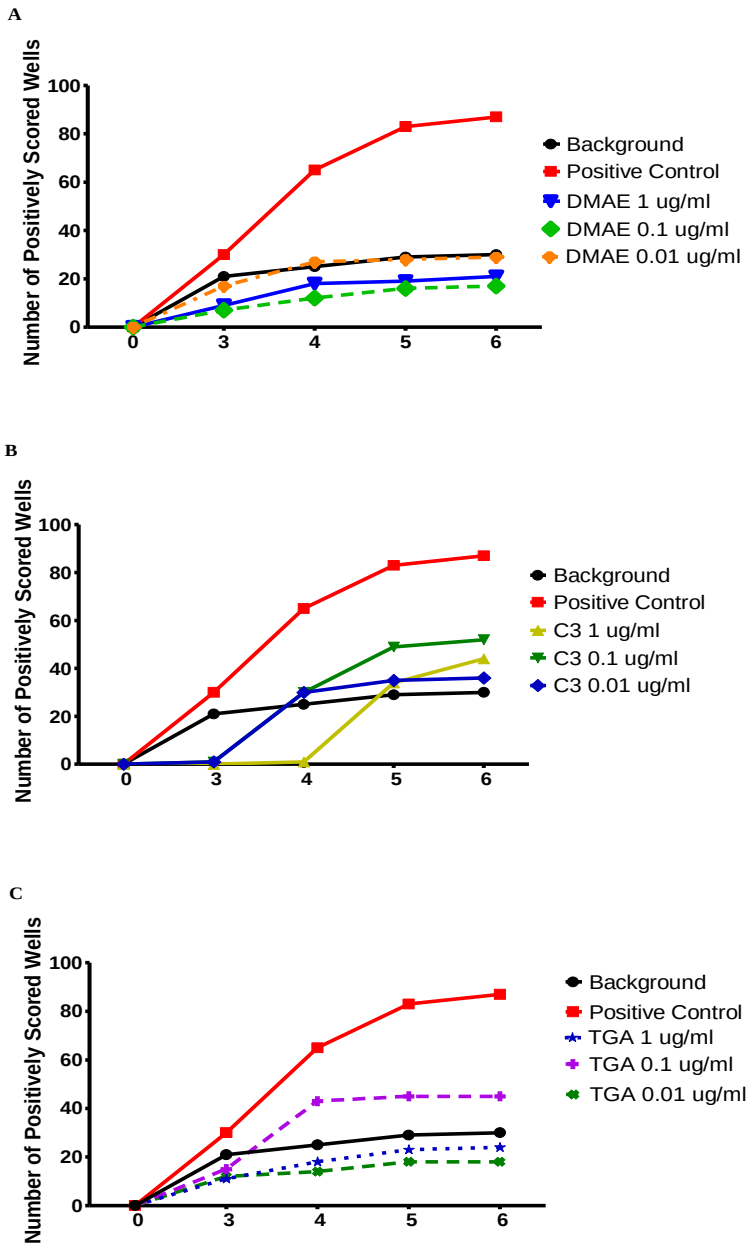

Figure 12. No genotoxic effects of fullerene derivatives using Bacterial Mutagenicity Assay. Assay shows the frequency of colonies formed proportional to the mutation frequency induced by fullerenes. All treatment groups did not show signs of mutagenic potential at dose concentrations (0.01 - 1.0 µg/ml).

To test the cytotoxicity of human skin tissue treated with fullerene derivatives, we measured LDH levels of tissue culture supernatant after two weeks of exposure. In Figure 13A, analysis indicated that DMAE 1.0µg/ml ($p<0.05$) and lower concentrations (0.01-0.1µg/ml) ($p<0.0001$) did not produce LDH levels above control. Results for C_3 (Figure 13B) were split with 1.0 and 0.01µg/ml ($p<0.05$) indicating little release of LDH, but mid concentration 0.1µg/ml ($p<0.0001$) caused far less LDH leakage in comparison to control and both high and low concentrations. Dose response of TGA (0.01 – 1.0µg/ml) remained consistent and highly significant ($P<0.001$) to prevent LDH exposure compared to control (Figure 13C).

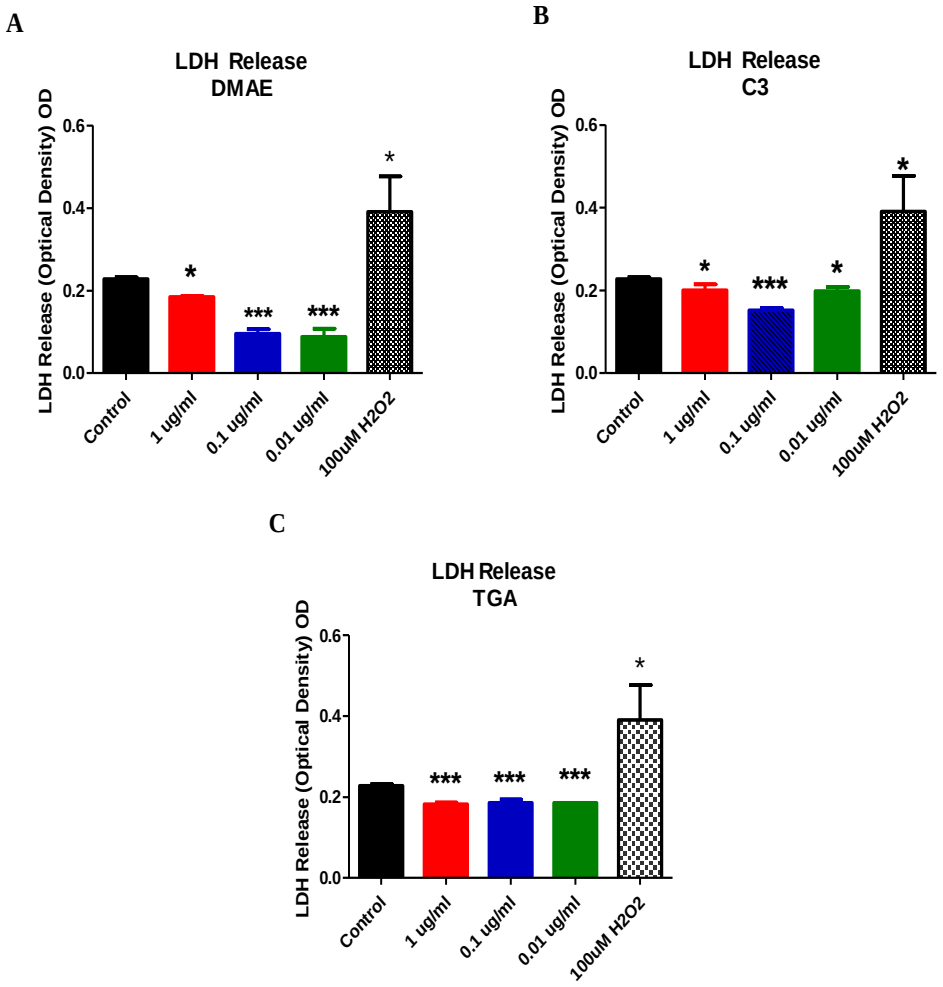

Figure 13. Reduction of Lactate Dehydrogenase enzyme by fullerenes. Cytotoxic effects of DMAE, C_3, and TGA concentrations (0.001 – 1.0µg.ml) suppressed LDH levels after two weeks of treatment. Results were expressed as mean ± SD. *p<0.05, **p<0.001, p<0.0001 comparing LDH release with control tissue.

Measurement of the metabolic activity (MTT) of fibroblasts in the presence of 1.0µg/ml TGA and 1µg/ml TGA/50µM H_2O_2 produced surprising results (Figure 14). TGA alone was found to increase metabolic activity after 30 minutes ($p<0.0001$) to 2 hours. After 2 hours of exposure fibroblasts decreased activity around 4 hours ($p<0.05$) and movement based on absorbance was not detected. Although not significant when

compared to control, 12 hour timepoint and beyond did result in increased metabolic activity. In contrast, 1µg/ml TGA in combination with 50µM H_2O_2 inhibited metabolic activity in fibroblasts across all timepoints ($p<0.001$) in comparison to control.

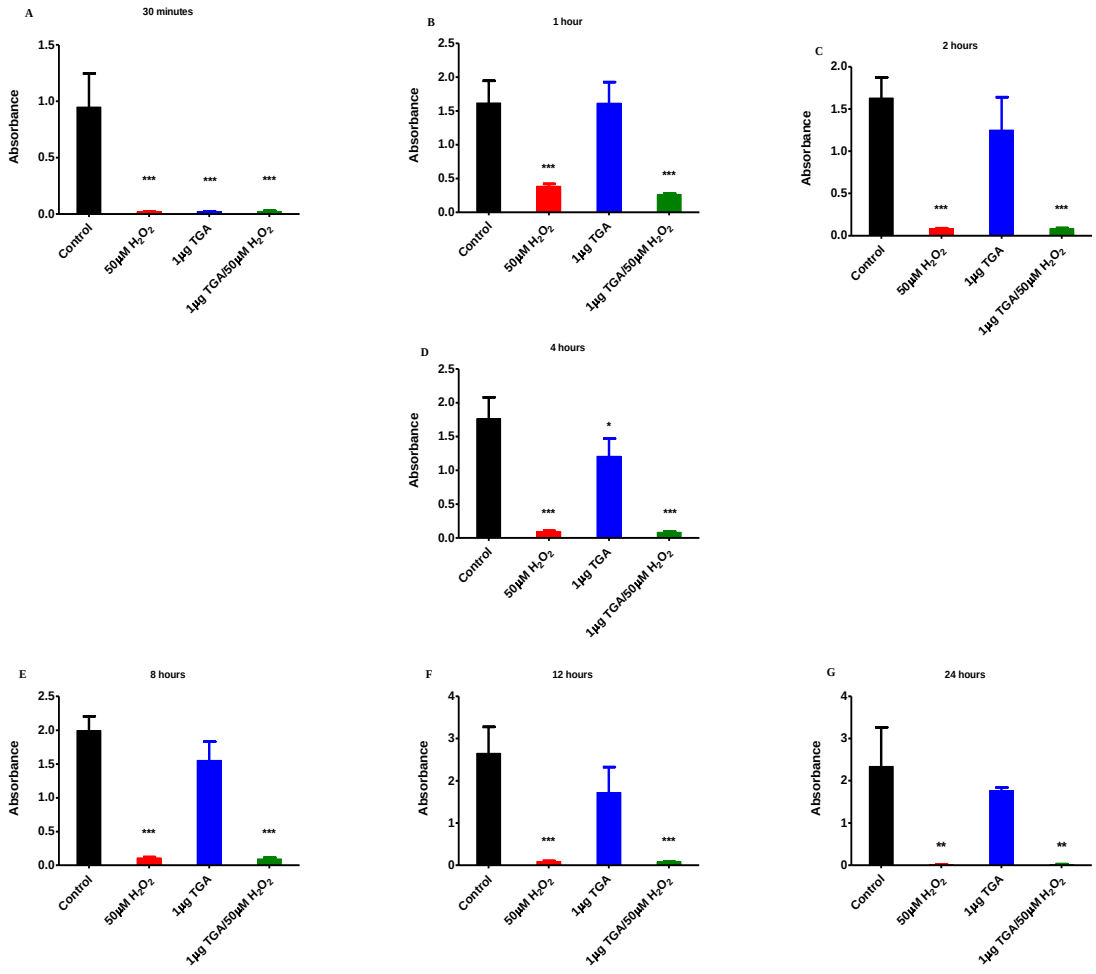

Figure 14. Metabolic activity of TGA increased at high concentration. Fibroblast cells metabolic activity measured after treatment with media (Control), 50µM H_2O_2, 1µg/ml TGA, and 1.0µg TGA/50µM H_2O_2 at the following timepoints: 30 minutes, 60 minutes, 2 hours, 4 hours, 8 hours, 12 hours, and 24 hours. Absorbance levels are mean ± SD, *$p<0.05$, **$p<0.001$, ***$p<0.0001$ by one-way ANOVA using Tukey post test.

The ability of TGA to sequester free radical production is important due their ability to cause inflammation leading to tissue damage. Reactive oxygen species are implicated in many oxidative stress related diseases and maintaining a homeostatic balance is ideal. After investigating the role of ROS generation in 3T3 cells after TGA exposure, preactivation presented no significance amongst groups (Appendix A). Percent change in ROS formation was calculated from preactivation against all remaining timepoints (0 minutes, 30 minutes, and 60 minutes), as represented in Figure 15.

Initial findings show at zero timepoint 0.01µg and 1.0µg TGA values were lower than controls, with 1.0µg TGA exhibiting ROS levels similar to L-ascorbic acid. However, upon increased exposure past zero timepoint; ROS formation decreases starting at 30 minutes and progressing to 60 minutes, both low and high concentrations of TGA decrease ROS production dramatically in fluorescence intensity. The highest amount of ROS formation was 50µM H_2O_2 (positive control) over all groups.

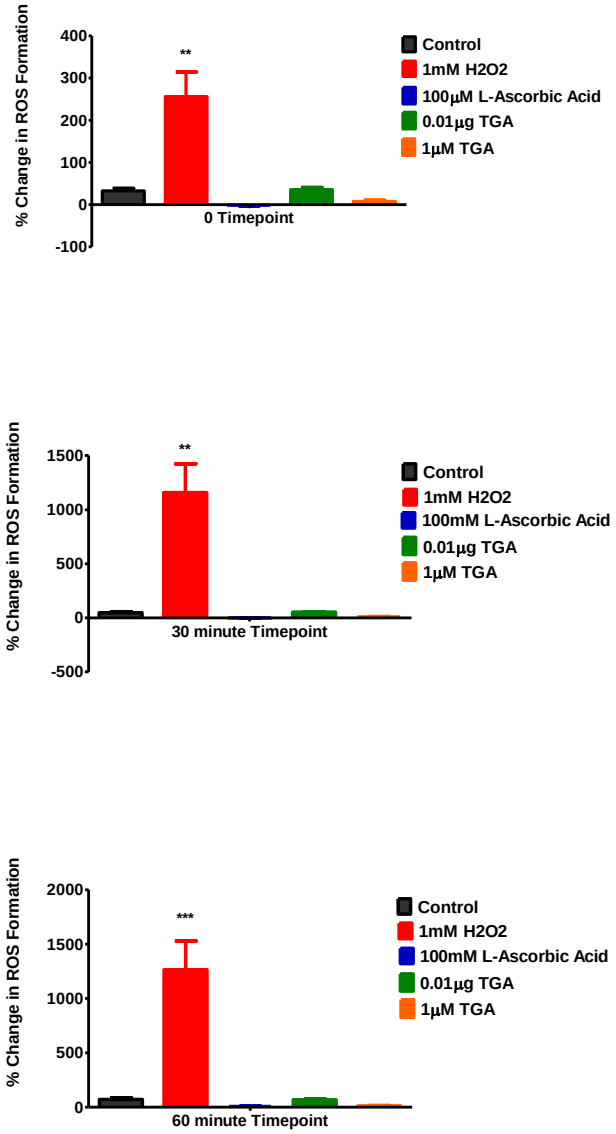

Figure 15. Percent change in ROS production by timepoints.
Fibroblast cells metabolic activity measured after treatment with media (Control), 100µM Vitamin C, 0.01µg TGA, and 1.0µg TGA at the following timpoints: 30 minutes, 60 minutes, 2 hours, 4 hours, 8 hours, 12 hours, and 24 hours. Absorbance levels are mean ± SD, **p<0.001, ***p<0.0001 by one-way ANOVA using Tukey post test.

To gage the ultraviolet (UV) protection of 0.01 and 1.0 µg.ml TGA concentrations on fibroblast cells, we examined it against known photo protectant and reactive oxygen intermediate, L-ascorbic acid and hydrogen peroxide, respectively. Cells

were pretreated for 24 hours and samples were rinsed prior to experiment. Figure 16, a low concentration of TGA (0.01- 1.0µg.ml) did not provide photo protection after 30 minutes ($p<0.0001$) of exposure reducing metabolic activity. Surprisingly, TGA at a higher concentration (1.0µg.ml) surpassed control and L-ascorbic acid after 30 minutes without UV exposure ($p<0.0001$), but no photo protection was observed after 30 minutes of UV exposure.

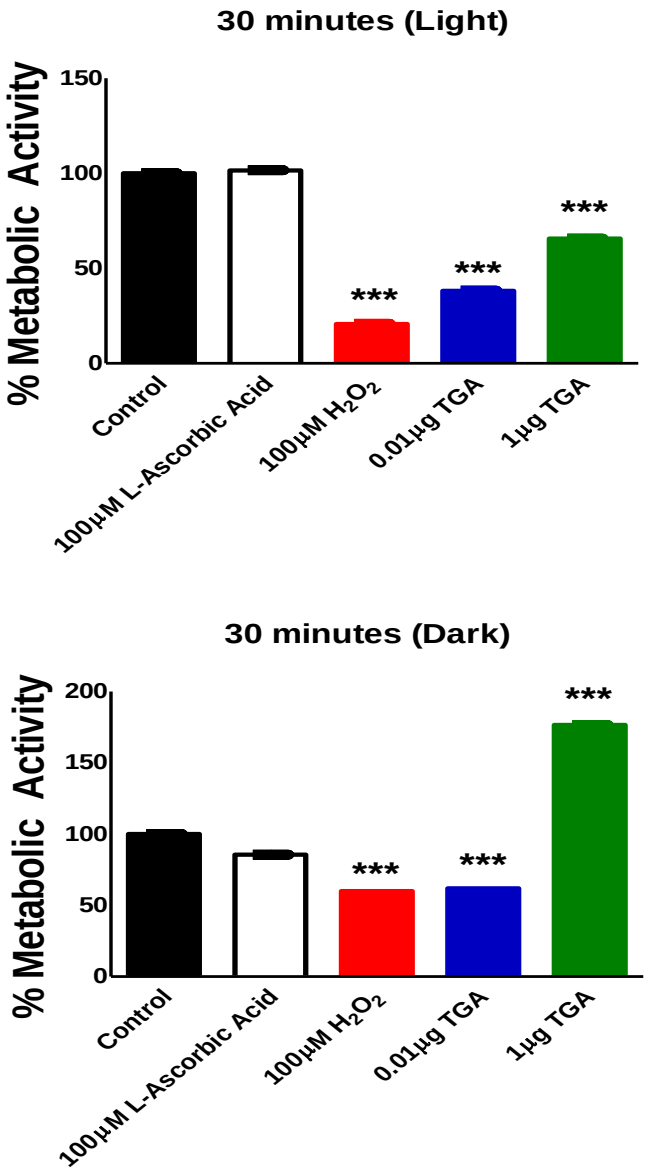

Figure 16. Effects of phototoxicity on fibroblasts treated with TGA. TGA (0.01 and 1.0µg/ml) inhibited metabolic activity after 30 minutes of UV exposure. Pre-incubation did increase metabolic activity without UV exposure for TGA 1.0µg/ml after 30 minutes. Values were expressed as mean ± SD. ***p<0.0001, comparing metabolic activity with control both in dark and UV exposed.

IV. 4 Conclusions

Safety assessment studies are paramount to understand the role fullerenes play in nanotoxicology. Here we investigated fundamental mechanisms leading to toxicity, such

as genotoxicity, cell death, and intracellular reactive oxygen species generation. Guidelines issued by the Food and Drug Administration (FDA), Cosmetic, Toiletry and Fragrance Association (CTFA) and the Organization for Economic Co-operation and Development (OECD) [141] are just a few battery of tests utilized in this study to address mechanisms of toxicity in fullerenes.

Mutagenicity assay, also known as the Ames test, was used to determine optimal dose concentrations for a series of fullerenes using *Salmonella typhimurium* strain as a reverse bacteria mutation assay. Bacterial reverse mutagenicity by functionalized fullerenes were examined on TA 100 histidine strain of *Salmonella typhimurium*; generally used to test mutagenicity of compounds due to their sensitive nature toward mutants of base pair substitutions. Dose concentrations (1- 0.01 µg/ml) did not show a significant increase in the number of bacterial reverse mutation colonies in *S. typhimurium* (TA 100) strain when compared to negative tests. As a result, functionalized fullerenes were determined not to induce DNA mutation under these conditions (Figure 12).

With regard to genotoxicity, Shinohara et al. examined C_{60} nanoparticles up to 1000 micrograms/ml and discovered no genotoxic effects using the Ames test in Chinese hamster cells [142]. However, some studies have presented genotoxic effects induced by fullerenes implicating oxidative stress, a major mechanism associated with redox imbalance between reactive oxygen species and antioxidants [143, 144]. Nonetheless, additional experiments will need to be conducted to assess DNA integrity in mammalian cell and tissue cultures.

Water soluble fullerenes were shown to lack mutagenic potential (Figure 12), but long term exposure on the body is of great concern. Here, we investigated the safety of three fullerene derivatuves (DMAE, C_3, and TGA) on human skin tissue ability to prevent or induce the enzyme lactate dehydrogenase after two weeks of treatment. The present study demonstrated significant dose response reduction of LDH in all three fullerene derivatives (Figure 13). Lactate dehydrogenase release was consistent across all concentrations (1.0 – 0.01µg/ml) for TGA in comparison to other groups. Cytotoxic effects of water soluble fullerenes have been well documented for inducing LDH release [145] but other studies have proven favorable safety profiles of fullerenes in biological systems [7, 43, 146]. Cytotoxicity data in this study supports previous literature findings of its ability to inhibit LDH. An ideal candidate to explore safety assessment and anti-aging effects was TGA, based on genotoxic and cytotoxic information in this study and efficacy studies in the previous section.

To establish the metabolic activity of fibroblast cells pre-treated with media, 50µM H_2O_2, 1.0µg.ml TGA, and 1.0µg.ml TGA/50µM H_2O_2 using a MTT assay. A time response study revealed a slow increase in cell growth for 1.0µg.ml TGA (Figure 14). The fullerene derivative, TGA, never exceeded cellular growth compared to control, but cellular growth was seen within this group (TGA 1.0µg.ml), intermittently. Initial metabolic activity levels of all groups at 30 minutes ($p<0.0001$) started below control group. But data analysis of 50µM H_2O_2 ($p<0.0001$) and 1.0µg.ml TGA/50µM H_2O_2 (combination) ($p<0.0001$) groups, revealed cellular activity remained below control and 1.0µg.ml TGA. A similar effect was seen with pristine C_{70} fullerenes exposed to human

keratinocytes and lung carcinoma cells at various concentrations. Cells exposed at 6 and 24 hours produced very small changes in cell viability [50]. The present results demonstrated TGA alone elicited increase in cellular metabolic activity, while combination inhibited metabolic activity in fibroblast cells under these condition.

Fullerenes have potential to act as potent biological antioxidants, by reacting with superoxide anions without being consumed [2]. However, fullerenes and other nanoparticles have been associated with toxicities through reactive oxygen species production. Reactive oxygen species induced by nanoparticles are usually followed by ROS cell-mediated tissue damage, immune cell activation, and inhibition of cell division and cell death [147].

Previous research of TGA inhibited airway inflammation and caused no acute toxicity in liver and kidney tissues in mice [8]. We investigated the inhibitory ability of low and high dose TGA concentrations, towards intracellular ROS formation in fibroblast cells. In this study, a time dependent decrease in ROS formation was noticed at high concentrations of TGA (Figure 15) in comparison to control. Percent change in ROS formation of control surpassed 1.0µg/ml TGA from 0-60 minutes timepoint. Inhibition of ROS by TGA (1.0µg/ml) produced effects similar to L-ascorbic acid. L-ascorbic acid, a potent water soluble antioxidant is biologically active, but unstable. This non-enzymatic defense mechanism helps to overturn ROS in healthy cells.

Pro-oxidants induced by nanoparticles can exhaust antioxidant reservoirs or produce intracellular ROS. Research suggest ROS can be both beneficial and detrimental to biological processes.[50, 148]. For example, PVP-fullerene diminished ROS over

ascorbic acid derivative in human skin keratinocytes, suggesting development as a rejuvenation cosmetic [149]. Liochev addressed the Free Radical Theory of Aging, noting how ROS can be the causative agents of aging but trigger pro survival signals in cells to extend lifespan[150]. An example of detrimental effect of ROS proved an increase in elastin mRNA levels in dermal fibroblasts, due to ROS imbalance resulted in photoaging of skin and inflammation [151]. Therefore, under these conditions TGA has potential as an effective inhibitor against ROS formation.

Antioxidants can either prevent initiation of free radicals or inactivate free radicals and can be depleted upon oxidant induced pathologies. Enzymatic (catalase and superoxide dismutase) and non-enzymatic (vitamin A, C, and E) antioxidants protect against photo damage in skin induced by ultraviolet exposure. Particular attention has been towards derivatives of C_{60} and C_{70} fullerenes impressive scavenging ability against ROS [137, 138, 152]. Our study showed significant ($p<0.0001$) decrease in metabolic activity at TGA (0.01-1.0µg/ml) after 30 minutes of UV exposure in comparison to control (Figure 16). However, 30 minutes of dark exposure, high concentration of TGA ($p<0.0001$) outperformed ascorbic acid, a known antioxidant used to prevent photoaging [151].

Literature review discovered a similar effect was seen in human lens epithelial cells and human retinal pigment epithelial cells using fullerol exposed to UVA resulted in a decrease in metabolic activity [145, 153]. Here the cytoprotective effects of TGA was unsuccessful in protection against UV exposure (decrease in metabolic activity), leading

to tissue damage. These results indicate a creative strategy to incorporate additional ROS-scavenging fullerenes or antioxidant to guard skin from deleterious stimuli.

CHAPTER V

PROTEOMIC EVALUATION ON BIOLOGICAL RESPONSE OF TGA

V. 1 Introduction

In the previous section, toxicology established TGA suppressed reactive oxygen species formation similar to L-ascorbic acid (Figure 15), but photo protection was not seen using TGA (Figure 16). Based on this information, TGA on some level, is analogous to an antioxidant's ability to combat ROS generation. Cellular toxicity was unaffected by TGA, but it does not explain mechanism of aging regarding fullerene/protein interactions.

Proteomics are widely used to interpret post translational modifications of fullerene and protein interaction in research. Interactions such as these, explains aging mechanisms at the protein level. Previous literature has shown the unusual effect nanomaterials have on biological systems due to their physicochemical modifications, particle size, and charge [154]. Nevertheless, compounded with the assortment of negative or positively charged and hydrophilic or hydrophobic nature of proteins; fullerenes have become prime targets in aging research. In one study, negatively charged fullerene derivatives induced pro-inflammatory cytokine TNF-α in macrophages, but positively charged fullerene derivatives were ineffective [155]. Hydrophobic or hydrophilic nature of fullerene derivatives can facilitate cellular effects through membrane manipulation [156].

Regulation of age and age related pathways manipulated by fullerene interaction, incorporates a complex arrangement of altering proteins producing both positive and negative outcomes. For instance, deletion of Rictor in keratinocytes increased lifespan, protected from senescence, and stress resistance in mitohormesis [157]; however dysregulation of TSC/mTOR contributes to tumor angiogenesis [158]. Our lab has reported the inhibitory effect of TGA on aging related disorder, inflammatory arthritis, suggesting it as a therapy against arthritis [7]. This study can provide insight into fullerene's ability to modulate protein expression along the mTOR pathway and its mediators.

V. 2 Methods

V. 2 .1 Fullerene Derivatives

TGA was purchased from Luna Innovations Incorporated (Danville, Va) [8, 9]. Characterization was done using matrix assisted laser desorption ionization mass spectrometry, nuclear magnetic resonance, and high performance liquid chromatography [44]. Z-average (mean value of the hydrodynamic diameter) of ~111.2 nm C_{70}-TGA (1μg/μl) in sterile water and the zeta potential was obtained by Nano-ZS Zetasizer NanoSeries with DTS software (Malvern Instruments, Zetasizer, NanoZS, Westborough, MA).

V. 2 .2 Cell Stress Protein Array

The expression profile of cell stress related proteins induced by two different fullerene derivatives (FD), C_3 and TGA. A protein array was performed using the Proteome Profiler Antibody Array kit (R&D Systems, Minneapolis, MN, USA)

according to manufacturer's instructions. Skin samples were treated with either C_3, TGA or untreated (control) for two weeks. Protein quantification was performed using a Bradford Assay and 300 µg proteins from each sample were incubated with the cell stress protein array overnight at 4°C. Cell stress membranes were quantified and image analysis by Bio Rad ChemiDoc (Bio Rad, Hercules, CA, USA) according to manufacturer's instructions.

V. 2 .3 Ex vivo Skin Model Treated with TGA and H_2O_2-mediated Activation

Human skin was obtained with informed consent from a 55 year old female, undergoing breast reduction from the Cooperative Human Tissue Network and approved by their Human Studies Institutional Review Board. Samples had excess fat removed and was placed in RPMI 1640 media (Life Technologies, Carlsbad, CA) supplemented with streptavidin and L-glutamine, 10% fetal bovine serum, HEPES, and amphotercin B for ~ 1.5 hours. Ex vivo human skin treated with TGA and activated with H_2O_2 (Figure 1), was placed in RPMI media and incubated at 37°C in 5% CO_2.

Tissue samples pretreated with RPMI media or fullerenes (N=16) — Day 1

WELLS	A	B	C	D
1	RPMI	RPMI + TGA	RPMI + H202	RPMI + H202 + TGA
2	RPMI	RPMI + TGA	RPMI + H202	RPMI + H202 + TGA
3	RPMI	RPMI + TGA	RPMI + H202	RPMI + H202 + TGA
4	RPMI	RPMI + TGA	RPMI + H202	RPMI + H202 + TGA

Day 2

WELLS	A	B	C	D
1	RPMI	RPMI + TGA	RPMI	RPMI + TGA
2	RPMI	RPMI + TGA	RPMI	RPMI + TGA
3	RPMI	RPMI + TGA	RPMI	RPMI + TGA
4	RPMI	RPMI + TGA	RPMI	RPMI + TGA

Day 3

Figure 17. Schematic diagram of experimental design. *Ex vivo* human skin pretreated with either TGA, 50μM H_2O_2 , or RPMI (Control) over three days. Protein lysates were used for protein array and western blot analysis.

The next day, skin samples were washed three times in phosphate buffered saline and immediately submerged into liquid nitrogen. All skin samples were placed in -80°C until further analysis. The dosage of 50 μM H_2O_2 was ideal for oxidative stress activation based on literature search [159]. Tissue samples were used for microarray and western blot analysis to determine TGA effect on protein modification.

V. 2 .4 Tissue Lysate Preparation and Antibody Protein Array

Skin tissue was rinsed three times with PBS then ~250mg of tissue was cut from sample. Tissue samples were homogenized on wet ice using a Bio-Gen Pro200 homogenzier (Pro Scientific, Oxford, CT). Samples were sonicated four times for 10 seconds in ice to shear nuclear DNA using a Beckman Microfuge R centrifuge (Beckman Coulter, Inc., Pasadena, CA). Supernatant was transferred to a new tube and protein was

quantified using Bradford assay (Bio Rad, Hercules, CA). All tissue lysates were placed immediately in -80^{0}C for further analysis by Kinexus™ Antibody Microarray Service.

Proteins potentially regulated in skin under the conditions above were investigated using a KAM-880 protein microarray as we have performed previously [160] (Kinexus Bioinformatics Corporation, Vancouver, BC), 50 µg of tissue lysate from each sample was covalently labeled with a fluorescent dye (Kinexus Bioinformatics proprietary methodology). Free dye molecules were removed by gel filtration, followed by blocking of non-specific sites on the array. Two samples (control and treated) are loaded on the sample chip in duplicate and incubated (details available at www.kinexus.ca). The Kinexus™ protein array profile was used to detect over 800 different antibodies. Unbound dye-labeled proteins were washed away and protein captured using a 16-bit laser array scanner (Perkin Elmer ScanArray Reader, Waltham, MA). Signal quantification measured using *ImaGene* 9.0 (BioDiscovery, El Sequndo, CA) and results were reported in Z scores (±1.2 – 1.5, significant), percent change from control (%CFC) and percent range in error and fold changes using globally normalized data as expressed spot intensity between control and treatment samples.

V. 2 .5 Protein Extraction and Western Blot Analysis

Skin samples were removed from -80^{0}C and ~0.1g – 0.2g frozen tissue was added to a 2ml microcentrifuge tube containing 1ml of RIPA Buffer (Boston BioProducts, Ashland, MA) and 10µl of protease inhibitor (Sigma-Aldrich, St. Louis, MO). Samples were homogenized using a Bio-Gen Pro200 homogenzier (Pro Scientific, Oxford, CT) on

ice. Samples were centrifuged at 16,000 g for 25 minutes and protein concentration determined using Bradford protein assay (BioRad, Hercules, CA).

For validation, 100 µg of protein derived from human skin was subjected to Western blot analysis. Samples were mixed with reducing buffer (0.125M Tris-HCl pH 6.8, 4% sodium dodecyl sulfate, 0.02% bromophenol blue, 10% β-mercapethanol, 20% glyercol) and heated to 95^0C for 5 minutes. Protein lysate were run in duplicate on 4-20% gradient SDS-PAGE gel (Invitrogen, Carlsbad, CA) and transferred onto a nitrocellulose membrane (Invitrogen, Carlsbad, CA). Membranes were blocked with LiCor blocking buffer (PBS) (Lincoln, NE) for 1 hour at room temperature, then probed with primary antibodies mTOR, RAPTOR, RICTOR (Cell Signaling, Danver, MA) diluted with 0.2% Tween 20 and LiCor blocking buffer for overnight incubation. Membrane was washed twice for ~10 minutes in PBST, and then probed using a secondary antibody label using an IR-Dye 670 or 800cw goat anti-rabbit or anti-mouse antibody mixed with 0.2% Tween 20 and blocking buffer for 1 hour at room temperature. Secondary antibodies were washed twice at 10 minutes, and then placed in PBS. Membranes were imaged wet using an Odyssey Imaging system (Lincoln, NE). Band intensity was measured by placing a box around bands and using the raw intensity values to quantify protein expression. β-actin (Sigma Aldrich, St. Louis, MO)was used as a background subtraction to determine protein expression levels.

Protein samples were imaged using chemiluminescent (ECL) and GE Amersham Imager 600 (Marlborough, MA). All protein extraction and preparation was same as above. Membranes were blocked with 5% nonfat dry milk and Tris-buffered saline

(TTBS) for 1 hour at room temperature, rinsed three times with TTBS, then probed with primary antibodies phospo mTOR, RAPTOR, RICTOR, SOD2, ATG13,pATG13 (Cell Signaling, Danver, MA) for overnight incubation. Membrane was washed three times for ~10 minutes in TTBS, and then probed using a secondary antibody label using anti-rabbit or anti-mouse antibody mixed with TTBS and 5% fetal bovine serum for 1 hour at room temperature. Secondary antibodies were washed three times at 10 minutes, and then placed in TTBS. Membranes were imaged using an Amersham Imaging 600 system (Marlborough, MA).

V. 2 .6 Statistical Analysis

The data used for these experiments DLS, ζ-potential, and western blot analysis was analyzed using GraphPad Prism 5.0 (San Diego, CA) and presented a mean ± SD. Data was analyzed by unpaired two-tailed t-test (comparison of two groups) or one-way ANOVA using Tukey's multiple comparison post hoc test (comparison of more than two groups). Significance was reported as a P-value < 0.05.

V. 3 Results

A cell stress protein array was used to detect 26 proteins associated with cellular stress. Tissue samples were treated for two weeks with C_3, TGA, or media (control). Superoxide dismutase 2 (SOD2), plays an important role in antioxidant defense against superoxide anion (O2-), in relation to, oxidative stress. As shown in Figure 17, C_3 and TGA decreased the expression of SOD 2 ($p<0.0001$) and thioredoxin 1 ($p<0.05$) by C_3 only, suggesting that proteins were under less duress. However, due to inconsistencies regarding protein arrays, western blot validation is necessary.

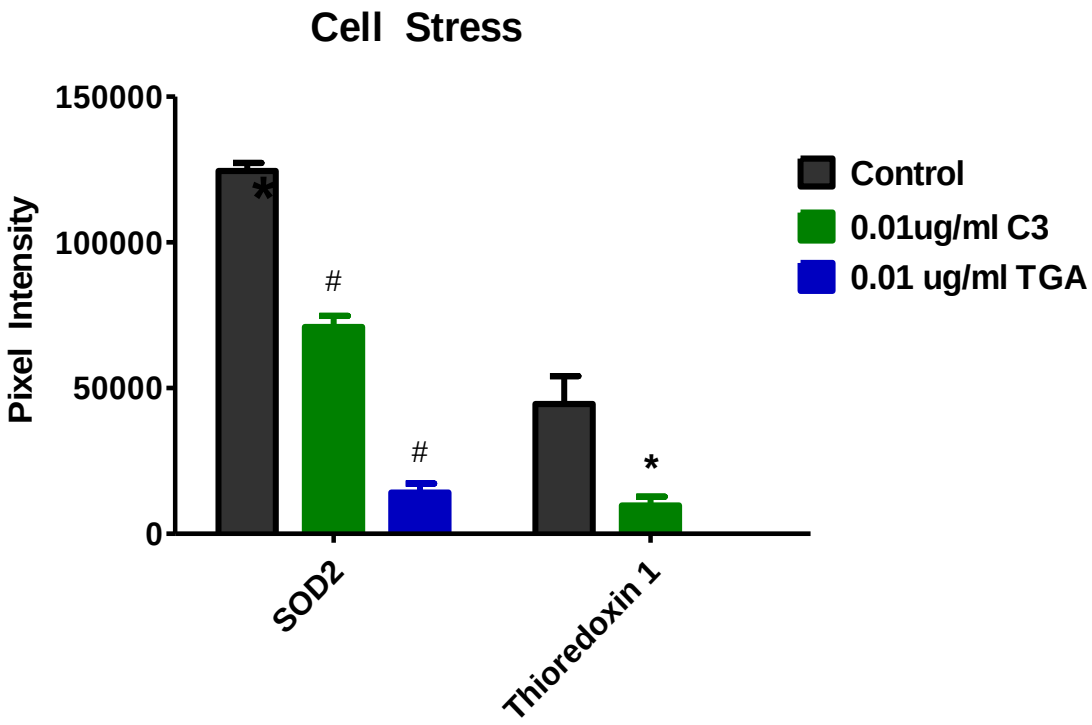

Figure 18. Fullerene Derivatives prevent upregulation of age-associated cell stress proteins. Human skin tissue was treated with or without fullerenes (0.01 µg/ml) and total protein extracted after two weeks. The protein extracts were examined for relative protein expression of 26 cell stress related proteins using a protein array (R&D Systems). Fullerene-treated skin samples significantly inhibited the upregulation of SOD2 and Thioredoxin 1. Mean ± SD taken in duplicates. * $p<0.05$, # $p<0.0001$.

To investigate the effects of TGA on oxidative stress-induced in human skin tissue was incubated with or without H_2O_2 following pre-incubation with TGA. The Kinexus™ protein microarray probed over 100 proteins including phosphorylated sites using 50µg of protein lysate. Approximately, 71 proteins were inhibited by 10% or more when tissue was pre-treated with TGA and activated with 50µM H_2O_2., in comparison to untreated based on percent change from control (%CFC) data (Appendix A, Table 2). Many of these proteins are linked to mTOR, a serine/threonine kinase, responsible for many health, disease, and aging related processes [161]. However, pre-incubation of

TGA prior to H_2O_2 challenge prevented the upregulation of several mTOR-related proteins. For example, S6K (ribosomal protein S6 kinase), a downstream effector, impaired adipocyte generation in mice fed a high fat diet (HFD)-induced obesity [162] as seen in Figure 19.

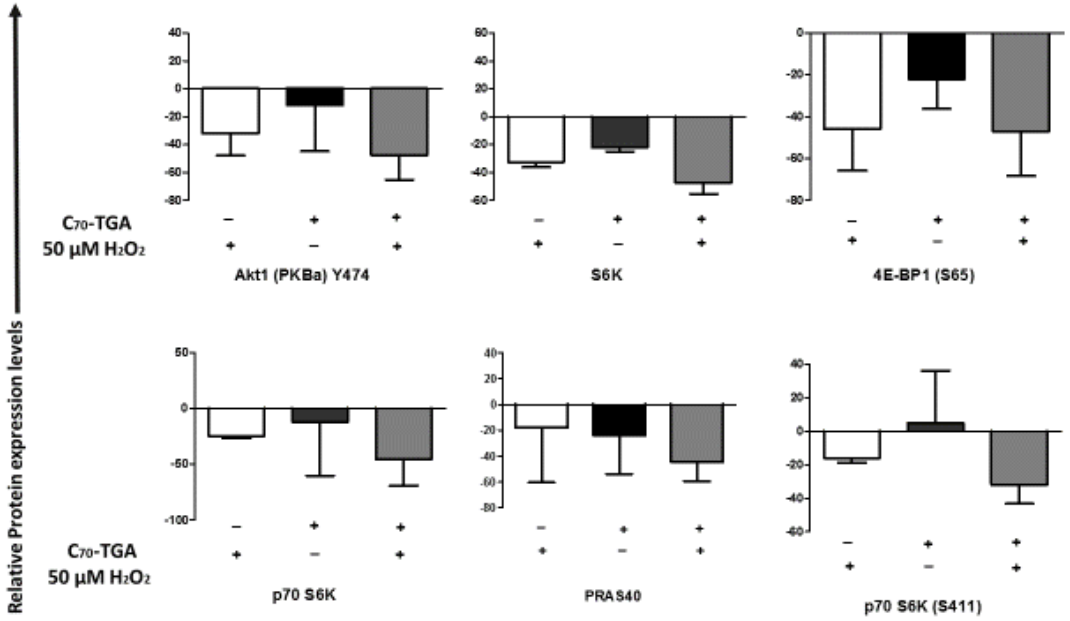

Figure 19. Inhibition of proteins associated with mTOR pathway treated with TGA and/or 50µM H_2O_2. Expression levels of Akt (PKBa-Y474), S6K, 4E-BP1 (S65), p70 S6K, PRAS40, and p70 S6K (S411). Kinexus protein microarray analysis using 50µg protein lysate to probe protein expression. Results expressed as relative protein expression levels using percent change from control (%CFC). Tissue lysate measured in duplicate. Tissues were pretreated with or without 1 µg.ml TGA overnight at 37°C/6% CO_2. The next day tissues were washed and challenged with (+) or without (-) hydrogen peroxide (50 µM) for 24 hours. Tissue lysate was used for protein isolation and protein microarray as described above or for Western blotting. Each condition was performed in quadruplicate. Shown is the mean relative intensities of each protein (±SD of four observed values) normalized against control. The black bar is the percent change in TGA treated tissues compared to hydrogen peroxide (white bar) treated tissues. The gray bar is the percent inhibition comparing FD pretreated and challenged tissues compared to non-FD treated hydrogen peroxide tissues.

An increase in total mTOR (43.74%) and pmTOR (S2448) (1.64%) for combination was seen over control levels (Figure 20) in samples treated over a three day

period. A few downstream effectors associated with the mTOR pathway were upregulated after pretreatment with TGA and activated with H_2O_2. In Figure 21, 4E-BP1 (2.28%), eIF4B (2.35%) and 4E-BP1 (T45) (6.53%) showed increased levels in skin tissue. These are a few proteins known as direct downstream effectors functioning as adaptor protein , protein kinase, or translation inhibitor along the mTOR pathway[163] [164]. Validation of key microarray protein results were conducted by western blot as an alternative approach to reduce false positives or negatives.

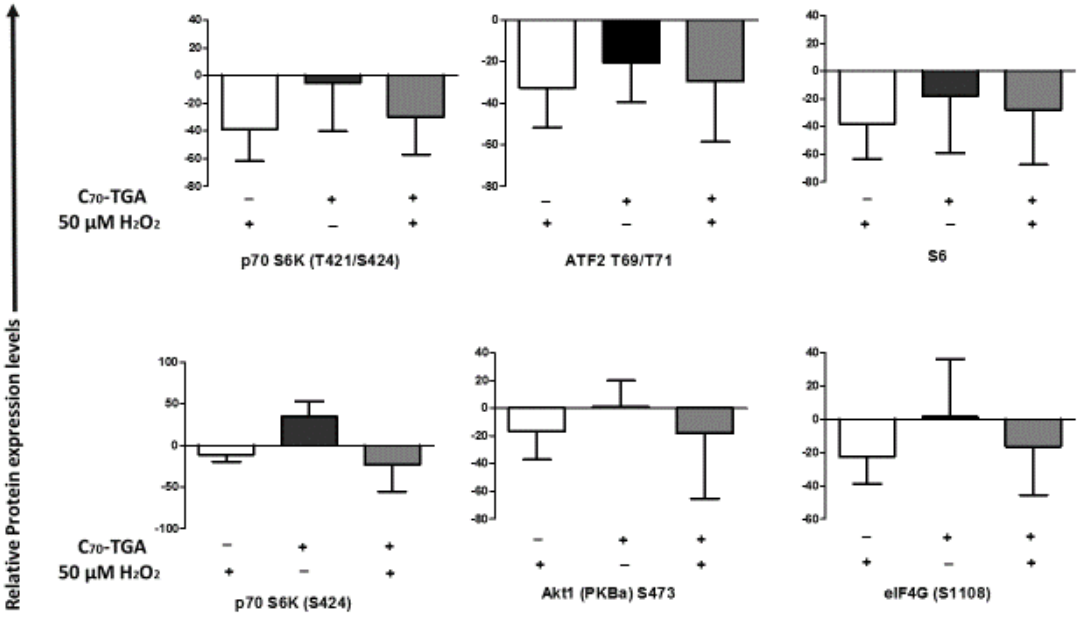

Figure 20. Inhibition of proteins associated with mTOR pathway treated with TGA and/or 50µM H_2O_2. Expression levels of p70 S6K (T421/S424), ATF2 (T69/T71), S6, p70 S6k (S424), AKT1 (PKBa) and S473 (eIFG (S1108). Kinexus protein microarray analysis using 50µg protein lysate to probe protein expression. Results expressed as relative protein expression levels using percent change from control (%CFC). Tissue lysate measured in duplicate. Tissues were pretreated with or without 1 µg.ml TGA overnight at 37°C/6% CO_2. The next day tissues were washed and challenged with (+) or without (-) hydrogen peroxide (50 µM) for 24 hours. Tissue lysate was used for protein isolation and protein microarray as described above or for Western blotting. Each condition was performed in quadruplicate. Shown is the mean relative intensities of each protein (±SD of four observed values) normalized against control. The black bar is the percent change in TGA treated tissues compared to hydrogen peroxide (white bar) treated tissues. The gray bar is the percent inhibition comparing FD pretreated and challenged tissues compared to non-FD treated hydrogen peroxide tissues.

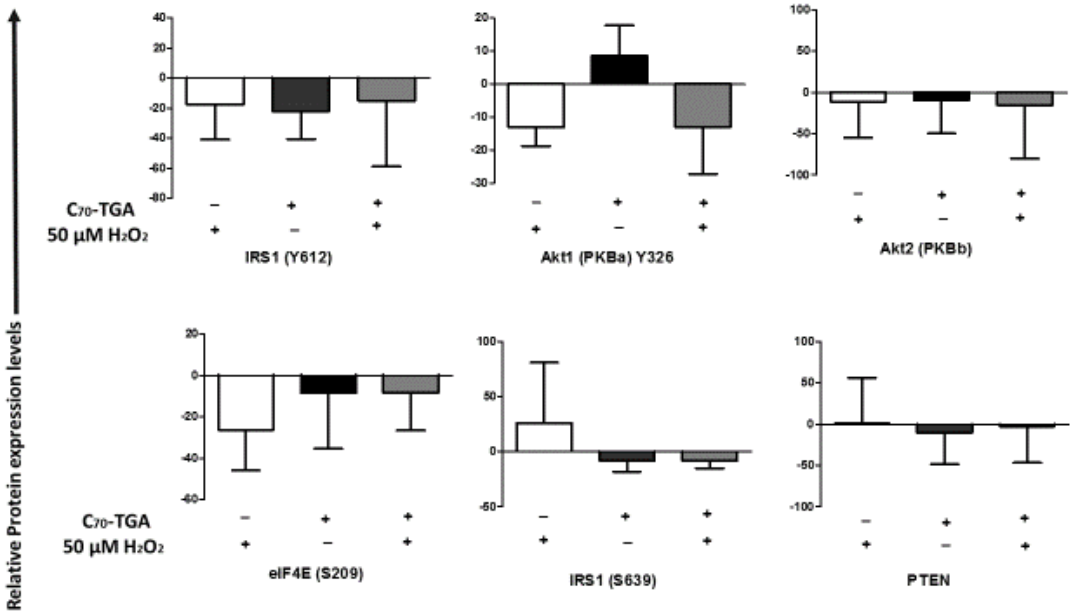

Figure 21. Inhibition of proteins associated with mTOR pathway treated with TGA and/or 50µM H_2O_2. Expression levels of IRS (Y612), AKT1 (PKBa) Y326, AKT2 (PKBb), eIF4E (S209), IRS1 (S639), and PTEN. Kinexus protein microarray analysis using 50µg protein lysate to probe protein expression. Results expressed as relative protein expression levels using percent change from control (%CFC). Tissue lysate measured in duplicate. Tissues were pretreated with or without 1 µg.ml TGA overnight at 37°C/6% CO_2. The next day tissues were washed and challenged with (+) or without (-) hydrogen peroxide (50 µM) for 24 hours. Tissue lysate was used for protein isolation and protein microarray as described above or for Western blotting. Each condition was performed in quadruplicate. Shown is the mean relative intensities of each protein (±SD of four observed values) normalized against control. The black bar is the percent change in TGA treated tissues compared to hydrogen peroxide (white bar) treated tissues. The gray bar is the percent inhibition comparing FD pretreated and challenged tissues compared to non-FD treated hydrogen peroxide tissues.

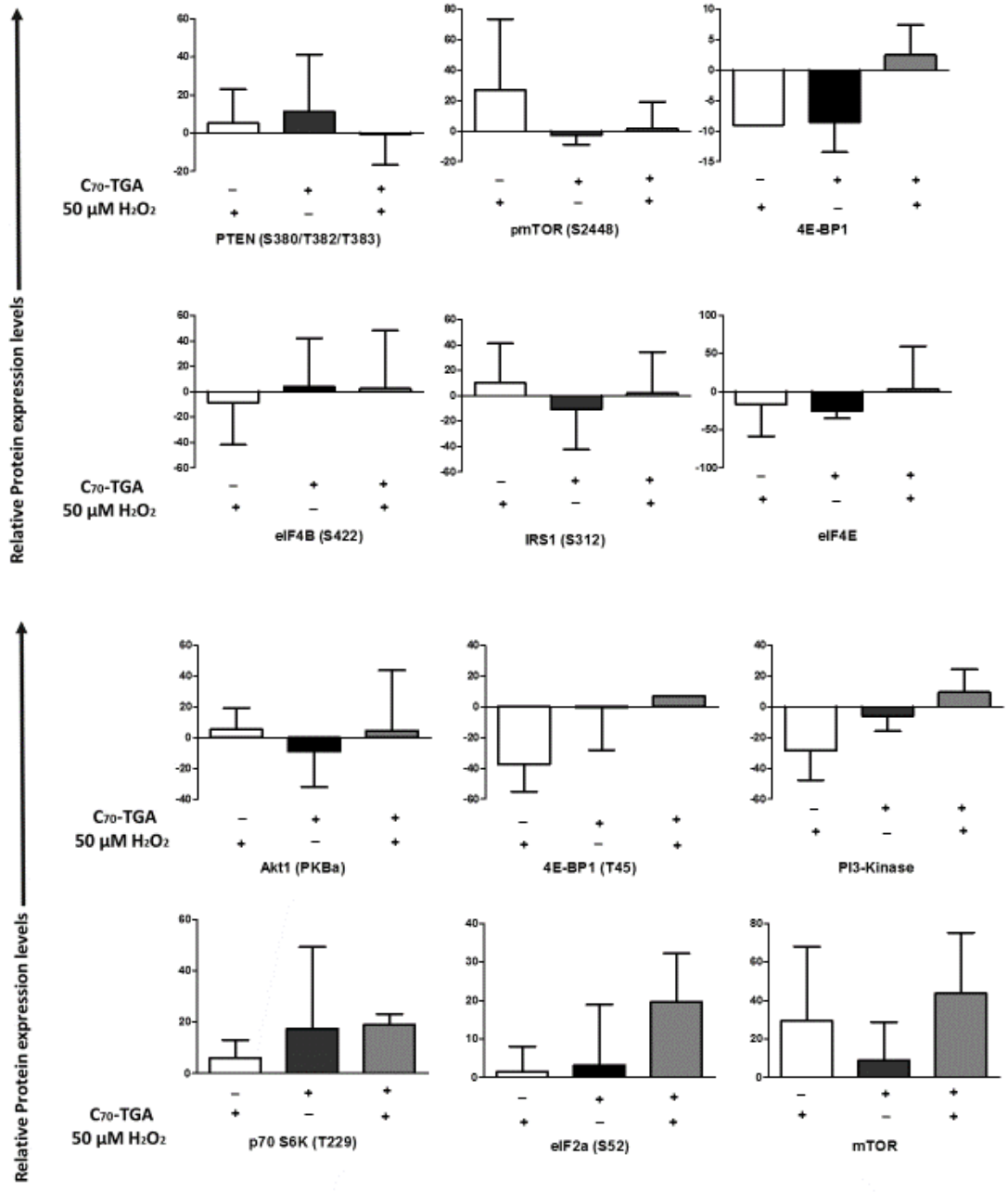

Figure 22. Down and upregulation of proteins associated with mTOR pathway treated with TGA and/or50µM H_2O_2. Expression levels of PTEN (S380/T382/T383), pmTOR. 4E-BP1, eIF4B (S422), IRS1 (S312), eIF4E, Akt1 (PKBa), 4E-BP1 (T45), PI3- Kinase, p70 S6K (T229), eIF2e (S52), and mTOR. Kinexus protein microarray analysis using 50µg protein lysate to probe protein expression. Results expressed as relative protein expression levels using percent change from control (%CFC). Tissues were pretreated with or without 1 µg.ml TGA overnight at 37°C/6% CO_2 . The next day tissues were washed and challenged with (+) or without (-) hydrogen peroxide (50 µM) for 24 hours. Tissue lysate was used for protein isolation and protein microarray as described above or for Western blotting. Each condition was performed in quadruplicate. Shown is the mean relative intensities of each protein (±SD of four observed

values) normalized against control. The black bar is the percent change in TGA treated tissues compared to hydrogen peroxide (white bar) treated tissues. The gray bar is the percent inhibition comparing FD pretreated and challenged tissues compared to non-FD treated hydrogen peroxide tissues.

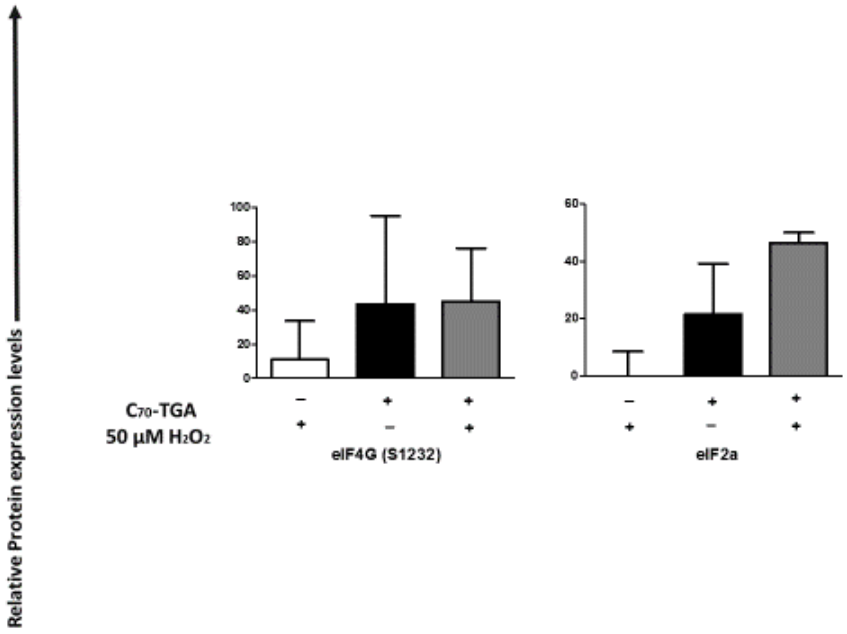

Figure 23. Upregulation of proteins associated with mTOR pathway treated with TGA and/or 50µM H_2O_2. Expression levels of eIF4G (S1232) and eIF2a. Kinexus protein microarray analysis using 50µg protein lysate to probe protein expression. Results expressed as relative protein expression levels using percent change from control (%CFC). Tissue lysate measured in duplicate. Tissues were pretreated with or without 1 µg.ml TGA overnight at 37°C/6% CO_2. The next day tissues were washed and challenged with (+) or without (-) hydrogen peroxide (50 µM) for 24 hours. Tissue lysate was used for protein isolation and protein microarray as described above or for Western blotting. Each condition was performed in quadruplicate. Shown is the mean relative intensities of each protein (±SD of four observed values) normalized against control. The black bar is the percent change in TGA treated tissues compared to hydrogen peroxide (white bar) treated tissues. The gray bar is the percent inhibition comparing FD pretreated and challenged tissues compared to non-FD treated hydrogen peroxide tissues.

Western blot analysis of tissue lysate was conducted to confirm the microarray data examining expression used in the protein array (Figures 19-23). mTOR protein levels did not show significant inhibition in either TGA or TGA-H_2O_2-challenged tissue samples compared control (Figure 24). This is a difference in protein microarray data of the previous section. Raptor (an mTOR-binding protein) was significantly inhibited

($p<0.0001$) when treated with TGA or TGA-H_2O_2-challenged treated cells over control group.

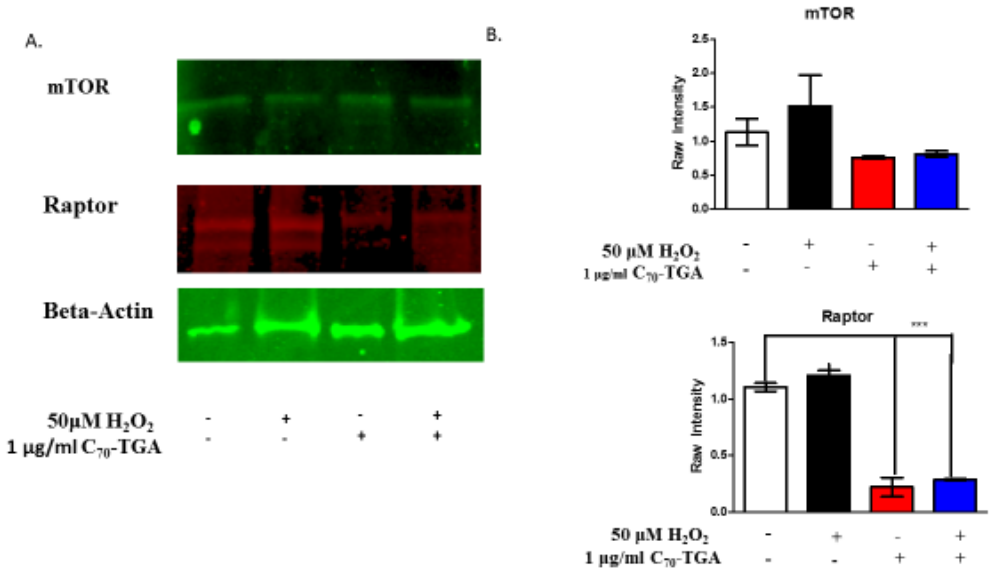

Figure 24. Western Blot analysis of mTOR and Raptor. A) Western blot analysis for validation of mTOR and Raptor protein levels. B) Quantification of mTOR and Raptor protein levels treated with 50 µM H_20_2 or 1 µg/ml TGA on human skin samples. Protein results represent the average protein expression and SEM of mTOR and Raptor, *** ($p<0.001$) highly significant changes in expression levels comparing all treatment groups to control.

Western blots were conducted using chemiluminescent due to equipment change during experimentation. In light of the role mTOR plays in aged skin, we investigated proteins associated with the mTOR complex. Protein expression was seen for mTOR in both TGA and TGA challenged with H_2O_2 (no significance); however, a down regulation was seen for RICTOR and RAPTOR (TGA, $p<0.05$ and TGA/H_2O_2, $p<0.01$) in comparison to control in Figure 25. ATG13 was downregulated in all treatment groups ($p<0.001$). Some slight differences was seen between protein microarray data and

western blot analysis. For example, pmTOR (S2448) microarray TGA was down regulated (-2.57%) but visually western blot presented a slight increase in change from control. A complete contradiction in analysis between microarray and western blot demonstrated a downregulation for both TGA and H_2O_2-challenged TGA for total mTOR (Figures 24 and 26), but upregulation in microarray(Figure 22).

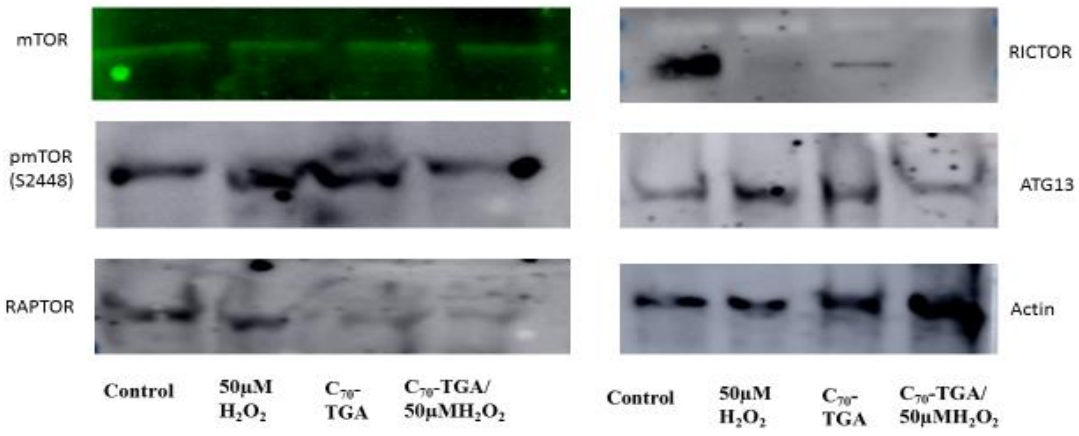

Figure 25. Western Blot analysis of proteins associated with the mTOR pathway. Results of western blot analysis of pMTOR (S2448), ATG13, SOD2, RICTOR, RAPTOR, and β-actin in human skin. Samples were treated on Day 1 with media (Lane 1), 50µM H_2O_2 (Lane 2), or TGA (Lane 3 and 4). Day 2-50µM H_2O_2 added to Lane 4. Day 3 all samples were removed for protein extraction. Lanes are represented as followed: Lane 1: Media only (control), Lane 2: 50µM H_2O_2, Lane 3: TGA, Lane 4: TGA and 50µM H_2O_2.

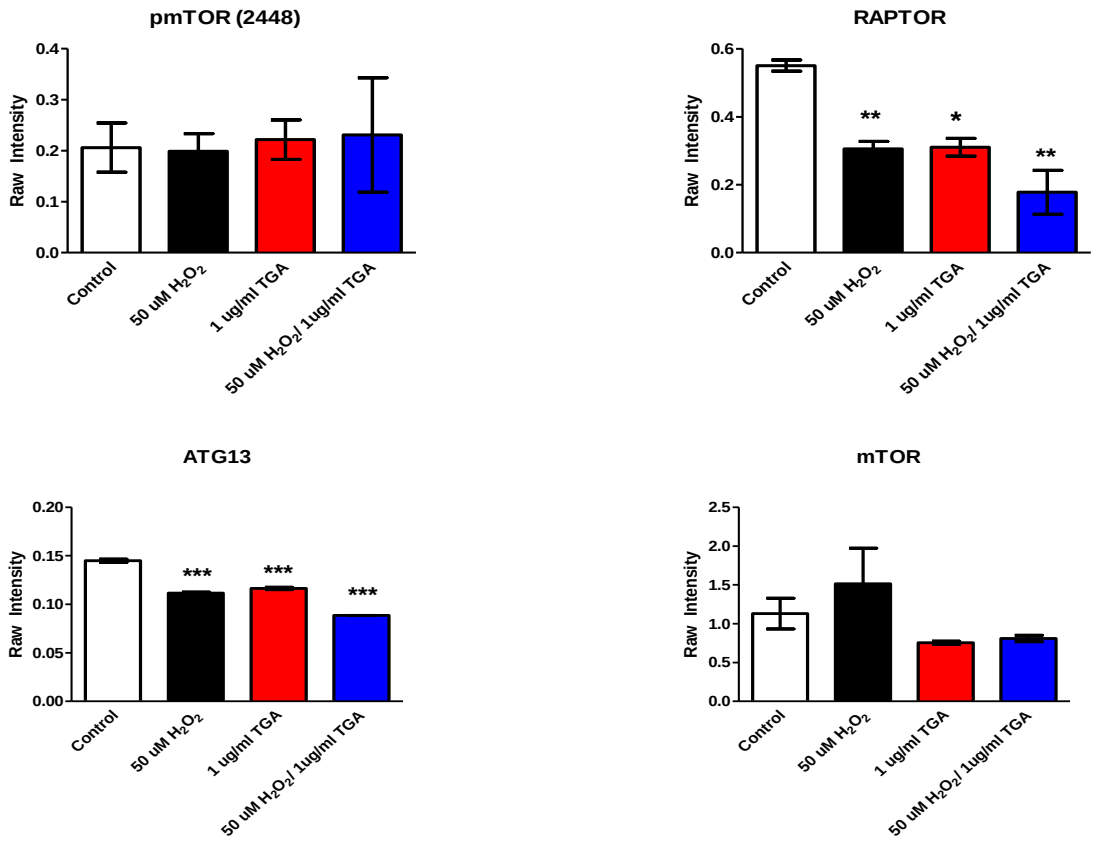

Figure 26. Densitometry of proteins associated with the mTOR pathway. Results of western blot analysis of pMTOR (S2448), ATG13, SOD2, RICTOR, RAPTOR, and β-actin in human skin. Samples were treated on Day 1 with media (Lane 1), 50µM H_2O_2 (Lane 2), or TGA (Lane 3 and 4). Day 2-50µM H_2O_2 added to Lane 4. Day 3 all samples were removed for protein extraction. Lanes are represented as followed: Lane 1: Media only (control), Lane 2: 50µM H_2O_2, Lane 3: TGA, Lane 4: TGA and 50µM H_2O_2.

Skin tissue was exposed to a pro-oxidant (50µM H_2O_2) to determine protein expression levels for superoxide dismutase 2. Densitometry was performed on chemiluminesence, due to fluorescence measurement unavailability. Previously, in Figure 18, a lower concentration of TGA (0.01µg) reduced SOD2 expression ($p<0.0001$) in human skin. Upon further investigation, TGA (1.0µg) lowered SOD2 protein expression (no significant), but H_2O_2-challenged TGA showed significance ($p<0.05$) over control in reducing antioxidant defense protein, SOD2 (Figure 27).

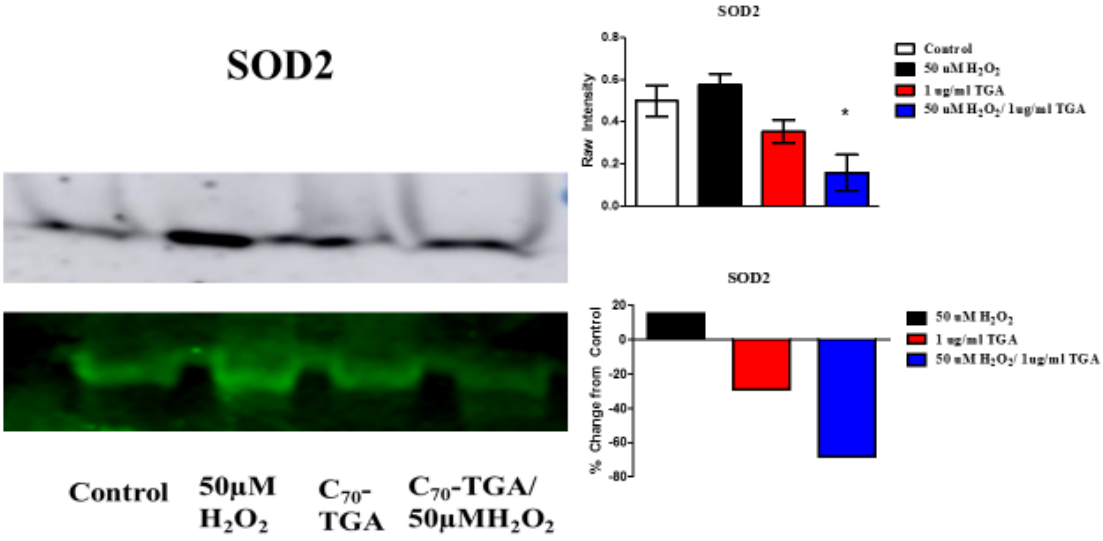

Figure 27. Inhibition of Superoxide Dismutase by TGA in Human Skin. Skin samples were treated over three days with either TGA, TGA and activated with 50µM H_2O_2, or untreated (Control) in a 24 well plate. Protein lysate was extracted and loaded into a 4-20% Tris-glycine gel. Protein expression levels of SOD2 inhibited by TGA in tissue, similar to expression seen in cells. Results depicted as mean ± SD, *p<0.05.

V. 4 Conclusion

In Figure 17, inhibition of cellular stress in protein lysate of human skin treated with C_3 or TGA in comparison to control. Previous results from toxicology assessment correlate with the lack of ROS generation, which support these findings at a protein level through the reduction of cellular antioxidants induced by fullerene derivatives. A significant attenuation of SOD2 ($p<0.0001$) by both TGA and C_3; while Thioredoxin 1 showed significance ($p<0.05$) for C_3, no expression was detected for TGA as a means to perform as a cellular defense mechanism.

Thus, we hypothesized that TGA could counteract oxidative stress-induced damage to human skin. For instance, previously we examined the effects of fullerene

derivatives on aged skin and discovered a thinning epidermis and induction of cellular stress response in SOD2 as well as ROS formation in control, while fullerene derivatives demonstrated an opposite effect. This and a previous study [165] has established these factors essential for understanding the aging process. These mechanisms are in place to alleviate deleterious effects of reactive oxygen species via enzymatic and/or non-enzymatic antioxidants. Previous studies have investigated SOD2 and mitochondria function related to aging and have shown that *tris*-malonic acid derivative of the fullerene C_{60} molecule (C_3) acts as a SOD2 mimic in *Sod2*$^{-/-}$ mice, which lack expression of mitochondrial manganese superoxide dismutase (MnSOD), increased their life span by 300% [4]. Nano-Pt has been shown to prolong worm lifespan in a dose-dependent removal of superoxide anion and hydrogen peroxide by resembling SOD2/catalase biologically [166].

Thioredoxin 1 expression is found in all mammalian cells and tissues, located in the nucleus, plasma membrane and protein secretion. To reduce ROS damage caused by mitochondrial respiration, thioredoxin 1 is utilized by mitochondrion and the nucleus requires the presence of reduced thioredoxin for transcription factor activation. Cytosolic thioredoxin controls cellular growth, apoptosis and inflammation. In the cytoplasmic regions of the cell is a regulator of cell signaling, stress, and transcription factors [167-170]. A study conducted by Young, et al., found suppression of thioredoxin 1 in human fibroblasts induced premature senescence by upregulating p53/p21 (Cip/Waf1) and p16 tumor suppressor pathways, in turn may enhance organismal longevity [171] because these pathways are believed to promote organism aging [172].

We have previously reported that fullerenes can counteract the effects of various ROS inducers including H_2O_2 [4, 8, 44] and reduce inflammatory mediator release from skin mast cells [44]. Upstream effectors of mTOR/Raptor complex such as: AKT, PI3K, and MAPK as well as downstream effectors S6 (S235/236), S6K1, and/or 4E-BP1/EIF4E are ideal targets for mitigating cellular aging [67]. Upregulation of mTOR by these effectors can lead to senescence and aging at both the cellular and organismal level. mTOR-related proteins that were significantly inhibited by TGA include Raptor (Figures 24 - 26). Our results in this study, follow a similar response in TGA treated samples effect on mTOR on aged skin. Lucafo and colleagues, reported fullerene treated MCF7 cells inhibited mTOR signaling through investigation of gene expression profiles [61]. These observations were similar with our lab experiments, and may suggest TGA may directly or indirectly influence the mammalian target of rapamycin (mTOR) pathway.

The current study suggests Raptor's role as a scaffolding protein connecting mTOR and phosphorylating substrates for mTOR activation [173]. The quantitative analysis of mTOR substrate signaling, only confirms translational levels, additional in-depth experiments to understand TGA interaction with the mTOR-Raptor complex are necessary to address the underlying molecular mechanisms. The selective mTOR inhibitor, rapamycin has been used as a positive control, to attenuate pathological defects in Alzheimer's mouse studies [174], while C_{60} fullerenes [43], and single walled carbon nanotubes [175] have been shown to inhibit mTOR activation. Little research has been conducted investigating the mTOR-Raptor complex and the effects of C_{70} to alter this pathway. Therefore, we can only conclude from previous studies focusing on the mTOR-

Raptor interaction, that show consistency with other mTOR inhibitor studies [176-178], to conclude that dissociation of Raptor from mTOR suppresses mTOR expression via TGA administration, thereby potentially suppressing cellular aging.

Potential target proteins were exposed using a Kinexus microarray to elucidate unknown mechanisms of aged skin treated with TGA or H_2O_2-challenged TGA. Another substrate of mTOR is S6, ribosomal protein S6 and 4E-BP1, plays a major role in cell proliferation, growth, and survival [179]. 4E-BP1 has several phosphorylation sites Thr46, Ser65, Thr70, Ser112, Sear 101, and Thr37[179, 180]; where Ser65 is more sensitive than Thr46[181]. These phospho sites are necessary for binding or dissociation of 4E-BP1-eIF4E complex. A dephosphorylation of 4E-BP1 and increase in eIF4E is correlated with environmental stress or infection [181, 182]. In this study, 4E-BP1 (S65) and (Thr46) was downregulated by TGA, whereas H_2O_2-challenged TGA upregulated 4E-BP1 (Thr46) and downregulated Ser65. A similar event was reported by Gingras et al., where Thr 46 was relatively insensitive to serum deprivation and rapamycin treatment, thereby blocking translation factor, eIF4E [181].

Activation of mTOR/S6/4E-BP1 leads to initiation of translation and cell growth, cellular senescence and aging[183]. Blocking of eIF4E and eIF4E (S209) was seen across both TGA and H_2O_2-challenged TGA (Appendix A, Table 2.), indicating even partial inhibition can impede eIF4E binding to 4E-BP1. Microarray data for S6 (Appendix A,

Table 2) produced a reduction in protein expression along with western blot analysis for mTOR/Raptor complex (Figure 24) suggesting a decrease in the aging process.

In contrast, others have argued the suppression of SOD2, inhibition of mTOR axis, and induction of autophagy have contributed to senescence, leading to accelerated aging [184]. Basal levels of cellular degradation (autophagy) are common to maintain cellular homeostasis, but accelerated levels are usually seen with enhanced ROS levels [185]. In the current study, ATG13, mTOR, and SOD2 levels were all diminished for both TGA and H_2O_2-challenged TGA (Figures 25, 25 and 27). It should be noted that autophagy is a cytoprotective process, not a destructive one. The role of mTOR and autophagy has been establish through various organisms[186, 187] Inhibition of mTOR triggers dephosphorylation of ATG13 allowing the formation of ATG13-ATG1 complex, but activation of mTOR phosphorylate ATG!3 preventing ATG1-ATG13 formation [185]. A few pieces of the puzzle is missing with this study and that is pATG13. This key component will verify whether TGA or combination can activate pmTOR to phosphorylate this protein preventing ATG13-ATG1 formation leading to autophagic initiation [185].

mTOR is a negative regulator of autophagy and inhibition under starvation conditions leads to induction of autophagy by means of activating mTOR/ATG13/ULK1/ULK2 [188]. A key component to longevity is caloric restriction, which can induce autophagy through inhibition of IGF (Insulin growth factors) and mTOR target [189]. In contrast, several researchers have noted that lifespan cannot be extended with caloric restriction if mTOR is suppressed as reported in worms, flies, and

yeast [189, 190]. Furthermore, inhibition of mTOR-Raptor (mTORC1) on protein translation was examined via S6K/4E-BP1/EIF4 complex where inhibition of S6k extended lifespan in mammals [191]. Although, an increase in autophagy was not seen in this study, it should be noted, normal levels of autophagy could suffice for removal of dysfunctional proteins if optimal numbers are maintained [188].

REFERENCES

1. Saathoff, J.G., et al., *In vitro toxicity assessment of three hydroxylated fullerenes in human skin cells.* Toxicol In Vitro, 2011. **25**(8): p. 2105-12.
2. Bakry, R., et al., *Medicinal applications of fullerenes.* Int J Nanomedicine, 2007. **2**(4): p. 639-49.
3. Tagmatarchis, N. and H. Shinohara, *Fullerenes in medicinal chemistry and their biological applications.* Mini Rev Med Chem, 2001. **1**(4): p. 339-48.
4. Ali, S.S., et al., *A biologically effective fullerene (C60) derivative with superoxide dismutase mimetic properties.* Free Radic Biol Med, 2004. **37**(8): p. 1191-202.
5. Dugan, L.L., et al., *Buckminsterfullerenol free radical scavengers reduce excitotoxic and apoptotic death of cultured cortical neurons.* Neurobiol Dis, 1996. **3**(2): p. 129-35.
6. Dellinger, A., et al., *Fullerene nanomaterials inhibit phorbol myristate acetate-induced inflammation.* Exp Dermatol, 2009. **18**(12): p. 1079-81.
7. Dellinger, A.L., et al., *Inhibition of Inflammatory Arthritis Using Fullerene Nanomaterials.* PLoS One, 2015. **10**(4): p. e0126290.
8. Norton, S.K., et al., *Epoxyeicosatrienoic acids are involved in the C(70) fullerene derivative-induced control of allergic asthma.* J Allergy Clin Immunol, 2012. **130**(3): p. 761-769 e2.
9. Zhou, Z., et al., *Liposomal formulation of amphiphilic fullerene antioxidants.* Bioconjug Chem, 2010. **21**(9): p. 1656-61.
10. Harman, D., *Aging: a theory based on free radical and radiation chemistry.* J Gerontol, 1956. **11**(3): p. 298-300.
11. Harman, D., *The biologic clock: the mitochondria?* J Am Geriatr Soc, 1972. **20**(4): p. 145-7.
12. Kharade, S.V., et al., *Mrg19 depletion increases S. cerevisiae lifespan by augmenting ROS defence.* FEBS Lett, 2005. **579**(30): p. 6809-13.
13. Radak, Z., H.Y. Chung, and S. Goto, *Exercise and hormesis: oxidative stress-related adaptation for successful aging.* Biogerontology, 2005. **6**(1): p. 71-5.
14. Bonawitz, N.D., et al., *Reduced TOR signaling extends chronological life span via increased respiration and upregulation of mitochondrial gene expression.* Cell Metab, 2007. **5**(4): p. 265-77.
15. Fabrizio, P., et al., *Regulation of longevity and stress resistance by Sch9 in yeast.* Science, 2001. **292**(5515): p. 288-90.
16. Bergfeld, W.F., *The aging skin.* Int J Fertil Womens Med, 1997. **42**(2): p. 57-66.
17. Farage, M.A., et al., *Intrinsic and extrinsic factors in skin ageing: a review.* Int J Cosmet Sci, 2008. **30**(2): p. 87-95.
18. Klaassen, C.D., L.J. Casarett, and J. Doull, *Casarett and Doull's toxicology : the basic science of poisons*. 8th ed. 2013, New York: McGraw-Hill Education. xiii, 1454 p.
19. Silberberg-Sinakin, I., et al., *Antigen-bearing Langerhans cells in skin, dermal lymphatics and in lymph nodes.* Cellular Immunology, 1976. **25**(2): p. 137-151.

20. Schuler, G., *Epidermal Langerhans cells*. 1991, Boca Raton: CRC Press. 324 p.
21. Moll, H., *The Immune functions of epidermal Langerhans cells*. Medical intelligence unit. 1995, New York Austin: Springer-Verlag ;R.G. Landes. 193 p.
22. Cichorek, M., et al., *Skin melanocytes: biology and development.* Advances in Dermatology and Allergology/Postępy Dermatologii I Alergologii, 2013. **30**(1): p. 30-41.
23. Winkelmann, R.K. and A.S. Breathnach, *THE MERKEL CELL.* J Investig Dermatol, 1973. **60**(1): p. 2-15.
24. Uchigasaki, S., H. Suzuki, and K. Inoue, *Merkel Cells in the Vellus Hair Follicles of Human Facial Skin: A Study Using Confocal Laser Microscopy.* The Journal of Dermatology, 2004. **31**(3): p. 218-222.
25. Tachibana, T., M. Endoh, and T. Nawa, *Immunohistochemical expression of G protein α-subunit isoforms in rat and monkey Merkel cell-neurite complexes.* Histochemistry and Cell Biology, 2001. **116**(3): p. 205-213.
26. Carlisle, K.S. and W. Montagna, *Aging Model for Unexposed Human Dermis.* J Investig Dermatol, 1979. **73**(1): p. 54-58.
27. Wang, E. and D. Gundersen, *Increased organization of cytoskeleton accompanying the aging of human fibroblasts in vitro.* Experimental Cell Research, 1984. **154**(1): p. 191-202.
28. Fonager, J., et al., *Mild stress-induced stimulation of heat-shock protein synthesis and improved functional ability of human fibroblasts undergoing aging in vitro.* Experimental Gerontology, 2002. **37**(10–11): p. 1223-1228.
29. JAUSLIN, M.L., et al., *Mitochondria-targeted antioxidants protect Friedreich Ataxia fibroblasts from endogenous oxidative stress more effectively than untargeted antioxidants.* The FASEB Journal, 2003. **17**(13): p. 1972-1974.
30. Aoshima, H., et al., *Safety evaluation of highly purified fullerenes (HPFs): based on screening of eye and skin damage.* The Journal of toxicological sciences, 2009. **34**(5): p. 555-562.
31. Plowden, J., et al., *Innate immunity in aging: impact on macrophage function.* Aging Cell, 2004. **3**(4): p. 161-167.
32. Zhang, X. and D.M. Mosser, *Macrophage activation by endogenous danger signals.* The Journal of pathology, 2008. **214**(2): p. 161-178.
33. Zhang, B., et al., *Macrophage apoptosis induced by aqueous C60 aggregates changing the mitochondrial membrane potential.* Environmental Toxicology and Pharmacology, 2015. **39**(1): p. 237-246.
34. Zhao, M., et al., *Dihydroquercetin (DHQ) ameliorated concanavalin A-induced mouse experimental fulminant hepatitis and enhanced HO-1 expression through MAPK/Nrf2 antioxidant pathway in RAW cells.* International Immunopharmacology, (0).
35. Barrett, D., et al., *Targeting the PI3K/AKT/mTOR signaling axis in children with hematologic malignancies.* Pediatric Drugs, 2012. **14**(5): p. 299-316.
36. Aljuffali, I.A., et al., *Cutaneous delivery of natural antioxidants: the enhancement approaches.* Curr Pharm Des, 2015. **21**(20): p. 2745-57.
37. Guterres, S.S., M.P. Alves, and A.R. Pohlmann, *Polymeric nanoparticles, nanospheres and nanocapsules, for cutaneous applications.* Drug Target Insights, 2007. **2**: p. 147-57.
38. Couvreur, P., et al., *Nanocapsule technology: a review.* Crit Rev Ther Drug Carrier Syst, 2002. **19**(2): p. 99-134.

39. Rijo, P., et al., *Antimicrobial plant extracts encapsulated into polymeric beads for potential application on the skin.* Polymers, 2014. **6**(2): p. 479-490.
40. Rigon, R., et al., *Skin Delivery and in Vitro Biological Evaluation of Trans-Resveratrol-Loaded Solid Lipid Nanoparticles for Skin Disorder Therapies.* Molecules, 2016. **21**(1): p. 116.
41. Mytych, J., M. Wnuk, and S.I.S. Rattan, *Low doses of nanodiamonds and silica nanoparticles have beneficial hormetic effects in normal human skin fibroblasts in culture.* Chemosphere, 2016. **148**: p. 307-315.
42. Monteiro-Riviere, N.A. and C.L. Tran, *Nanotoxicology : progress toward nanomedicine*. Second edition. ed. xix, 492 p.
43. Dugan, L.L., et al., *Carboxyfullerene neuroprotection postinjury in Parkinsonian nonhuman primates.* Ann Neurol, 2014. **76**(3): p. 393-402.
44. Norton, S.K., et al., *A new class of human mast cell and peripheral blood basophil stabilizers that differentially control allergic mediator release.* Clin Transl Sci, 2010. **3**(4): p. 158-69.
45. Isobe, H., et al., *Nonviral gene delivery by tetraamino fullerene.* Mol Pharm, 2006. **3**(2): p. 124-34.
46. Ryman-Rasmussen, J.P., J.E. Riviere, and N.A. Monteiro-Riviere, *Penetration of intact skin by quantum dots with diverse physicochemical properties.* Toxicol Sci, 2006. **91**(1): p. 159-65.
47. Kroto, H.W., *The stability of the fullerenes Cn, with n = 24, 28, 32, 36, 50, 60 and 70.* Nature, 1987. **329**(6139): p. 529-531.
48. Jensen, A.W., S.R. Wilson, and D.I. Schuster, *Biological applications of fullerenes.* Bioorg Med Chem, 1996. **4**(6): p. 767-79.
49. Zhang, Y., et al., *Influences of acid-treated multiwalled carbon nanotubes on fibroblasts: proliferation, adhesion, migration, and wound healing.* Ann Biomed Eng, 2011. **39**(1): p. 414-26.
50. Horie, M., et al., *In vitro evaluation of cellular influences induced by stable fullerene C70 medium dispersion: Induction of cellular oxidative stress.* Chemosphere, 2013. **93**(6): p. 1182-1188.
51. Harhaji, L., et al., *Modulation of tumor necrosis factor-mediated cell death by fullerenes.* Pharm Res, 2008. **25**(6): p. 1365-76.
52. Bianco, A., et al., *Biomedical applications of functionalised carbon nanotubes.* Chemical Communications, 2005(5): p. 571-577.
53. Cui, Y., et al., *Biomimetic peptide nanosensors.* Accounts of Chemical Research, 2012. **45**(5): p. 696-704.
54. Moon, T.C., et al., *Advances in mast cell biology: New understanding of heterogeneity and function.* Mucosal Immunology, 2010. **3**(2): p. 111-128.
55. Fukuoka, Y., et al., *Human skin mast cells express complement factors C3 and C5.* J Immunol, 2013. **191**(4): p. 1827-34.
56. Cadenas, C., R. Marchan, and J.G. Hengstler, *Buckyballs (fullerenes): free radical sponges or inflammatory agents?* Arch Toxicol, 2012. **86**(12): p. 1807-8.
57. Quick, K.L., et al., *A carboxyfullerene SOD mimetic improves cognition and extends the lifespan of mice.* Neurobiology of Aging, 2008. **29**(1): p. 117-128.

58. Hwang, K.C. and D. Mauzerall, *Photoinduced electron transport across a lipid bilayer mediated by C70.* Nature, 1993. **361**(6408): p. 138-40.
59. Aschberger, K., et al., *Review of carbon nanotubes toxicity and exposure--appraisal of human health risk assessment based on open literature.* Crit Rev Toxicol, 2010. **40**(9): p. 759-90.
60. Baker, J., et al., *Structure and properties of C70.* Chemical Physics Letters, 1991. **184**(1–3): p. 182-186.
61. Lucafò, M., et al., *Profiling the molecular mechanism of fullerene cytotoxicity on tumor cells by RNA-seq.* Toxicology, 2013. **314**(1): p. 183-192.
62. Jiang, X., et al., *RNase non-sensitive and endocytosis independent siRNA delivery system: delivery of siRNA into tumor cells and high efficiency induction of apoptosis.* Nanoscale, 2013. **5**(16): p. 7256-64.
63. Salazar-Salinas, K., C. Kubli-Garfias, and J.M. Seminario, *Computational design of a CNT carrier for a high affinity bispecific anti-HER2 antibody based on trastuzumab and pertuzumab Fabs.* J Mol Model, 2013. **19**(7): p. 2797-810.
64. Dellinger, A.L., Z. Zhou, and C.L. Kepley, *A steroid-mimicking nanomaterial that mediates inhibition of human lung mast cell responses.* Nanomedicine, 2014. **10**(6): p. 1185-93.
65. Zoncu, R., A. Efeyan, and D.M. Sabatini, *mTOR: from growth signal integration to cancer, diabetes and ageing.* Nat Rev Mol Cell Biol, 2011. **12**(1): p. 21-35.
66. Parkhitko, A.A., et al., *Kinase mTOR: regulation and role in maintenance of cellular homeostasis, tumor development, and aging.* Biochemistry (Mosc), 2014. **79**(2): p. 88-101.
67. Hay, N. and N. Sonenberg, *Upstream and downstream of mTOR.* Genes Dev, 2004. **18**(16): p. 1926-45.
68. Easton, J.B. and P.J. Houghton, *mTOR and cancer therapy.* Oncogene, 2006. **25**(48): p. 6436-46.
69. Jacinto, E., et al., *Mammalian TOR complex 2 controls the actin cytoskeleton and is rapamycin insensitive.* Nat Cell Biol, 2004. **6**(11): p. 1122-8.
70. Sarbassov, D.D., et al., *Rictor, a novel binding partner of mTOR, defines a rapamycin-insensitive and raptor-independent pathway that regulates the cytoskeleton.* Curr Biol, 2004. **14**(14): p. 1296-302.
71. Peterson, T.R., et al., *DEPTOR is an mTOR inhibitor frequently overexpressed in multiple myeloma cells and required for their survival.* Cell, 2009. **137**(5): p. 873-86.
72. Kaizuka, T., et al., *Tti1 and Tel2 are critical factors in mammalian target of rapamycin complex assembly.* J Biol Chem, 2010. **285**(26): p. 20109-16.
73. Kim, D.H., et al., *mTOR interacts with raptor to form a nutrient-sensitive complex that signals to the cell growth machinery.* Cell, 2002. **110**(2): p. 163-75.
74. Wiza, C., E.B.M. Nascimento, and D.M. Ouwens, *Role of PRAS40 in Akt and mTOR signaling in health and disease*. Vol. 302. 2012. E1453-E1460.
75. Lamming, D.W., et al., *Depletion of Rictor, an essential protein component of mTORC2, decreases male lifespan.* Aging Cell, 2014. **13**(5): p. 911-7.
76. Oh, W.J. and E. Jacinto, *mTOR complex 2 signaling and functions.* Cell Cycle, 2011. **10**(14): p. 2305-16.
77. Pearce, L.R., et al., *Identification of Protor as a novel Rictor-binding component of mTOR complex-2.* Biochem J, 2007. **405**(3): p. 513-22.

78. Woo, S.Y., et al., *PRR5, a novel component of mTOR complex 2, regulates platelet-derived growth factor receptor beta expression and signaling.* J Biol Chem, 2007. **282**(35): p. 25604-12.
79. Gilley, R., et al., *Adaptation to chronic mTOR inhibition in cancer and in aging.* Biochem Soc Trans, 2013. **41**(4): p. 956-61.
80. Wullschleger, S., R. Loewith, and M.N. Hall, *TOR signaling in growth and metabolism.* Cell, 2006. **124**(3): p. 471-484.
81. Laplante, M. and D.M. Sabatini, *MTOR signaling in growth control and disease.* Cell, 2012. **149**(2): p. 274-293.
82. Perl, A., *mTOR activation is a biomarker and a central pathway to autoimmune disorders, cancer, obesity, and aging.* Ann N Y Acad Sci, 2015.
83. Yang, L., et al., *The mTORC1 effectors S6K1 and 4E-BP play different roles in CNS axon regeneration.* Nat Commun, 2014. **5**: p. 5416.
84. Robida-Stubbs, S., et al., *TOR signaling and rapamycin influence longevity by regulating SKN-1/Nrf and DAF-16/FoxO.* Cell Metab, 2012. **15**(5): p. 713-24.
85. Jacinto, E., et al., *Mammalian TOR complex 2 controls the actin cytoskeleton and is rapamycin insensitive.* Nature Cell Biology, 2004. **6**(11): p. 1122-1128.
86. Zinzalla, V., et al., *Activation of mTORC2 by association with the ribosome.* Cell, 2011. **144**(5): p. 757-68.
87. Pearce, L.R., D. Komander, and D.R. Alessi, *The nuts and bolts of AGC protein kinases.* Nature Reviews Molecular Cell Biology, 2010. **11**(1): p. 9-22.
88. Sarbassov, D.D., et al., *Phosphorylation and regulation of Akt/PKB by the rictor-mTOR complex.* Science, 2005. **307**(5712): p. 1098-101.
89. Lamming, D.W., et al., *Rapamycin-induced insulin resistance is mediated by mTORC2 loss and uncoupled from longevity.* Science, 2012. **335**(6076): p. 1638-43.
90. Albert, V. and M.N. Hall, *mTOR signaling in cellular and organismal energetics.* Current Opinion in Cell Biology, 2015. **33**(0): p. 55-66.
91. Kato, S., et al., *Evaluation of biological responses to polymeric biomaterials by RT-PCR analysis. II: Study of HSP 70 mRNA expression.* J Biomater Sci Polym Ed, 1997. **8**(10): p. 809-14.
92. Li, Y., et al., *Age-Associated Increase of Skin Fibroblast-Derived Prostaglandin E2 Contributes to Reduced Collagen Levels in Elderly Human Skin.* J Invest Dermatol, 2015.
93. Bergeron, Y., et al., *mTOR signaling contributes to motor skill learning in mice.* Front Mol Neurosci, 2014. **7**: p. 26.
94. Santini, E., T.N. Huynh, and E. Klann, *Mechanisms of translation control underlying long-lasting synaptic plasticity and the consolidation of long-term memory.* Prog Mol Biol Transl Sci, 2014. **122**: p. 131-167.
95. Madison, K.C., et al., *Lamellar granule extrusion and stratum corneum intercellular lamellae in murine keratinocyte cultures.* J Invest Dermatol, 1988. **90**(2): p. 110-6.
96. Norlen, L. and A. Al-Amoudi, *Stratum corneum keratin structure, function, and formation: the cubic rod-packing and membrane templating model.* J Invest Dermatol, 2004. **123**(4): p. 715-32.
97. Fitzpatrick, T.B. and K. Wolff, *Fitzpatrick's dermatology in general medicine*. 7th ed. 2008, New York: McGraw-Hill Medical.

98. Barbero, A.M. and H.F. Frasch, *Transcellular route of diffusion through stratum corneum: results from finite element models.* J Pharm Sci, 2006. **95**(10): p. 2186-94.
99. Subedi, R.K., et al., *Recent advances in transdermal drug delivery.* Arch Pharm Res, 2010. **33**(3): p. 339-51.
100. Nohynek, G.J., E.K. Dufour, and M.S. Roberts, *Nanotechnology, cosmetics and the skin: is there a health risk?* Skin Pharmacol Physiol, 2008. **21**(3): p. 136-49.
101. Schneider, M., et al., *Nanoparticles and their interactions with the dermal barrier.* Dermatoendocrinol, 2009. **1**(4): p. 197-206.
102. Barry, B.W., *Novel mechanisms and devices to enable successful transdermal drug delivery.* European Journal of Pharmaceutical Sciences, 2001. **14**(2): p. 101-114.
103. Cevc, G., et al., *The skin: a pathway for systemic treatment with patches and lipid-based agent carriers.* Adv Drug Deliv Rev, 1996. **18**(3): p. 349-378.
104. Baroli, B., et al., *Penetration of Metallic Nanoparticles in Human Full-Thickness Skin.* Journal of Investigative Dermatology, 2007. **127**(7): p. 1701-1712.
105. Xia, X.R., N.A. Monteiro-Riviere, and J.E. Riviere, *Skin penetration and kinetics of pristine fullerenes (C60) topically exposed in industrial organic solvents.* Toxicol Appl Pharmacol, 2010. **242**(1): p. 29-37.
106. Souto, G.D., A.R. Pohlmann, and S.S. Guterres, *Ultraviolet A Irradiation Increases the Permeation of Fullerenes into Human and Porcine Skin from C₆₀-Poly(vinylpyrrolidone) Aggregate Dispersions.* Skin Pharmacol Physiol, 2015. **28**(1): p. 22-30.
107. Dugan, L.L., et al., *Carboxyfullerenes as neuroprotective agents.* Proc Natl Acad Sci U S A, 1997. **94**(17): p. 9434-9439.
108. Garber, C.A. and C. Nightingale, *Characterizing cosmetic effects and skin morphology by scanning electron microscopy.* J Soc Cosmet Chem, 1976. **27**: p. 509-531.
109. Grossman, R., *The role of dimethylaminoethanol in cosmetic dermatology.* Am J Clin Dermatol, 2005. **6**(1): p. 39-47.
110. Liu, S., et al., *Effects of Dimethylaminoethanol and Compound Amino Acid on D-Galactose Induced Skin Aging Model of Rat.* The Scientific World Journal, 2014. **2014**: p. 507351.
111. Proksch, E., et al., *Bathing in a magnesium-rich Dead Sea salt solution improves skin barrier function, enhances skin hydration, and reduces inflammation in atopic dry skin.* Int J Dermatol, 2005. **44**(2): p. 151-7.
112. Batheja, P., et al., *Topical drug delivery by a polymeric nanosphere gel: Formulation optimization and in vitro and in vivo skin distribution studies.* Journal of Controlled Release, 2011. **149**(2): p. 159-67.
113. Ali, S.S., J.I. Hardt, and L.L. Dugan, *SOD Activity of carboxyfullerenes predicts their neuroprotective efficacy: a structure-activity study.* Nanomedicine: Nanotechnology, Biology, and Medicine, 2008. **4**(4): p. 283-294.
114. Quick, K.L., et al., *A carboxyfullerene SOD mimetic improves cognition and extends the lifespan of mice.* Neurobiol Aging, 2008. **29**(1): p. 117-28.
115. Sayes, C.M., et al., *The differential cytotoxicity of water-soluble fullerenes.* Nano Letters, 2004. **4**(10): p. 1881-1887.
116. El-Domyati, M., et al., *Electro-optical Synergy Technique: A New and Effective Nonablative Approach to Skin Aging.* J Clin Aesthet Dermatol, 2010. **3**(12): p. 22-30.

117. Arif, T. and M. Adil, *Nanotechnology-Dermatological Perspective.* Int J Nanomed Nanosurg, 2016. **2**(2).
118. Tiwary, A.K., B. Sapra, and S. Jain, *Innovations in transdermal drug delivery: formulations and techniques.* Recent patents on drug delivery & formulation, 2007. **1**(1): p. 23-36.
119. Truong, A.B. and P.A. Khavari, *Control of keratinocyte proliferation and differentiation by p63.* Cell Cycle, 2007. **6**(3): p. 295-299.
120. Leite-Silva, V.R., et al., *The effect of formulation on the penetration of coated and uncoated zinc oxide nanoparticles into the viable epidermis of human skin in vivo.* European Journal of Pharmaceutics and Biopharmaceutics, 2013. **84**(2): p. 297-308.
121. Nohynek, G.J., et al., *Grey goo on the skin? Nanotechnology, cosmetic and sunscreen safety.* Crit Rev Toxicol, 2007. **37**(3): p. 251-77.
122. Hagens, W.I., et al., *What do we (need to) know about the kinetic properties of nanoparticles in the body?* Regulatory Toxicology and Pharmacology, 2007. **49**(3): p. 217-229.
123. Kusaka, T., et al., *Effect of Silica Particle Size on Macrophage Inflammatory Responses.* PLoS ONE, 2014. **9**(3): p. e92634.
124. Moddaresi, M., et al., *Effects of lipid nanocarriers on the performance of topical vehicles in vivo.* J Cosmet Dermatol, 2009. **8**(2): p. 136-43.
125. Saathoff, J.G., et al., *In vitro toxicity assessment of three hydroxylated fullerenes in human skin cells.* Toxicology in Vitro, 2011. **25**(8): p. 2105-2112.
126. Jovanović, B., et al., *Hydroxylated fullerenes inhibit neutrophil function in fathead minnow (Pimephales promelas Rafinesque, 1820).* Aquatic Toxicology, 2011. **101**(2): p. 474-482.
127. Rouse, J.G., et al., *Effects of mechanical flexion on the penetration of fullerene amino acid-derivatized peptide nanoparticles through skin.* Nano Lett, 2007. **7**(1): p. 155-60.
128. Park, E.-J., et al., *Carbon fullerenes (C60s) can induce inflammatory responses in the lung of mice.* Toxicol Appl Pharmacol, 2010. **244**(2): p. 226-233.
129. Vidanapathirana, A.K., et al., *PVP formulated fullerene (C60) increases Rho-kinase dependent vascular tissue contractility in pregnant Sprague Dawley rats.* Reproductive Toxicology, 2014. **49**: p. 86-100.
130. Ershova, E.S., et al., *Toxic and DNA damaging effects of a functionalized fullerene in human embryonic lung fibroblasts.* Mutation Research/Genetic Toxicology and Environmental Mutagenesis, 2016. **805**: p. 46-57.
131. Zeynalov, E.B., N.S. Allen, and N.I. Salmanova, *Radical scavenging efficiency of different fullerenes C60–C70 and fullerene soot.* Polymer Degradation and Stability, 2009. **94**(8): p. 1183-1189.
132. Ali, S.S., J.I. Hardt, and L.L. Dugan, *SOD activity of carboxyfullerenes predicts their neuroprotective efficacy: a structure-activity study.* Nanomedicine, 2008. **4**(4): p. 283-94.
133. Liu, Q., et al., *C70-Carboxyfullerenes as Efficient Antioxidants to Protect Cells against Oxidative-Induced Stress.* ACS Applied Materials & Interfaces, 2013. **5**(21): p. 11101-11107.
134. Ehrich, M., et al., *Fullerene antioxidants decrease organophosphate-induced acetylcholinesterase inhibition in vitro.* Toxicology in Vitro, 2011. **25**(1): p. 301-307.

135. Uttara, B., et al., *Oxidative stress and neurodegenerative diseases: A review of upstream and downstream antioxidant therapeutic options.* Current Neuropharmacology, 2009. **7**(1): p. 65-74.
136. Valko, M., et al., *Free radicals and antioxidants in normal physiological functions and human disease.* International Journal of Biochemistry and Cell Biology, 2007. **39**(1): p. 44-84.
137. Dugan, L.L., et al., *Fullerene-based antioxidants and neurodegenerative disorders.* Parkinsonism Relat Disord, 2001. **7**(3): p. 243-246.
138. Xiao, L., et al., *The water-soluble fullerene derivative 'Radical Sponge®'exerts cytoprotective action against UVA irradiation but not visible-light-catalyzed cytotoxicity in human skin keratinocytes.* Bioorganic & medicinal chemistry letters, 2006. **16**(6): p. 1590-1595.
139. Markovic, Z. and V. Trajkovic, *Biomedical potential of the reactive oxygen species generation and quenching by fullerenes (C60).* Biomaterials, 2008. **29**(26): p. 3561-3573.
140. Dhawan, A., et al., *Stable colloidal dispersions of C60 fullerenes in water: Evidence for genotoxicity.* Environmental Science and Technology, 2006. **40**(23): p. 7394-7401.
141. Katz, L.M., K. Dewan, and R.L. Bronaugh, *Nanotechnology in cosmetics.* Food and Chemical Toxicology, 2015. **85**: p. 127-137.
142. Shinohara, N., et al., *In vitro and in vivo genotoxicity tests on fullerene C60 nanoparticles.* Toxicol Lett, 2009. **191**(2-3): p. 289-96.
143. Toyokuni, S., *Oxidative stress and cancer: The role of redox regulation.* Biotherapy, 1998. **11**(2-3): p. 147-154.
144. Benameur, L., et al., *DNA damage and oxidative stress induced by CeO2 nanoparticles in human dermal fibroblasts: Evidence of a clastogenic effect as a mechanism of genotoxicity.* Nanotoxicology, 2015. **9**(6): p. 696-705.
145. Wielgus, A.R., et al., *Phototoxicity and cytotoxicity of fullerol in human retinal pigment epithelial cells.* Toxicol Appl Pharmacol, 2010. **242**(1): p. 79-90.
146. Niwa, Y. and N. Iwai, *Genotoxicity in cell lines induced by chronic exposure to water-soluble fullerenes using micronucleus test.* Environ Health Prev Med, 2006. **11**(6): p. 292-7.
147. Robbins, S.L., V. Kumar, and R.S. Cotran, *Robbins and Cotran pathologic basis of disease*. 8th ed. 2010, Philadelphia, PA: Saunders/Elsevier. xiv, 1450 p.
148. Fidanzi-Dugas, C., et al., *Analysis of the in vitro and in vivo effects of Photodynamic Therapy on Prostate Cancer by using new photosensitizers, protoporphyrin IX-polyamine derivatives.* Biochim Biophys Acta, 2017.
149. Xiao, L., et al., *Antioxidant effects of water-soluble fullerene derivatives against ultraviolet ray or peroxylipid through their action of scavenging the reactive oxygen species in human skin keratinocytes.* Biomed Pharmacother, 2005. **59**(7): p. 351-8.
150. Liochev, S.I., *Reactive oxygen species and the free radical theory of aging.* Free Radical Biology and Medicine, 2013. **60**: p. 1-4.
151. Traikovich, S.S., *Use of topical ascorbic acid and its effects on photodamaged skin topography.* Arch Otolaryngol Head Neck Surg, 1999. **125**(10): p. 1091-8.
152. Kato, S., et al., *Fullerene-C 60 incorporated in liposome exerts persistent hydroxyl radical-scavenging activity and cytoprotection in UVA/B-irradiated keratinocytes.* J Nanosci Nanotechnol, 2011. **11**(5): p. 3814-3823.

153. Roberts, J.E., et al., *Phototoxicity and cytotoxicity of fullerol in human lens epithelial cells.* Toxicol Appl Pharmacol, 2008. **228**(1): p. 49-58.
154. Verma, A. and F. Stellacci, *Effect of surface properties on nanoparticle-cell interactions.* Small, 2010. **6**(1): p. 12-21.
155. Xiang, K., et al., *Cytotoxicity and TNF-α secretion in RAW264.7 macrophages exposed to different fullerene derivatives.* J Nanosci Nanotechnol, 2012. **12**(3): p. 2169-2178.
156. Akhtar, M.J., et al., *Mechanism of ROS scavenging and antioxidant signalling by redox metallic and fullerene nanomaterials: Potential implications in ROS associated degenerative disorders.* Biochimica et Biophysica Acta (BBA) - General Subjects, 2017. **1861**(4): p. 802-813.
157. Tassone, B., et al., *Rictor/mTORC2 deficiency enhances keratinocyte stress tolerance via mitohormesis.* Cell Death Differ, 2017.
158. Lee, D.-F., et al., *IKKβ Suppression of TSC1 Links Inflammation and Tumor Angiogenesis via the mTOR Pathway.* Cell. **130**(3): p. 440-455.
159. Stone, J.R. and S. Yang, *Hydrogen peroxide: a signaling messenger.* Antioxid Redox Signal, 2006. **8**(3-4): p. 243-70.
160. Ryan, J.J., et al., *Fullerene nanomaterials inhibit the allergic response.* J Immunol, 2007. **179**(1): p. 665-72.
161. Laplante, M. and David M. Sabatini, *mTOR Signaling in Growth Control and Disease.* Cell. **149**(2): p. 274-293.
162. Carnevalli, L.S., et al., *S6K1 Plays a Critical Role in Early Adipocyte Differentiation.* Dev Cell. **18**(5): p. 763-774.
163. Choo, A.Y., et al., *Rapamycin differentially inhibits S6Ks and 4E-BP1 to mediate cell-type-specific repression of mRNA translation.* Proceedings of the National Academy of Sciences, 2008. **105**(45): p. 17414-17419.
164. Grammer, T.C., et al., *The p70S6K signalling pathway: a novel signalling system involved in growth regulation.* Cancer Surv, 1996. **27**: p. 271-92.
165. Velarde, M.C., et al., *Mitochondrial oxidative stress caused by Sod2 deficiency promotes cellular senescence and aging phenotypes in the skin.* Aging (Albany NY), 2012. **4**(1): p. 3-12.
166. Kim, J., et al., *Effects of a potent antioxidant, platinum nanoparticle, on the lifespan of Caenorhabditis elegans.* Mechanisms of Ageing and Development, 2008. **129**(6): p. 322-331.
167. Lillig, C.H. and A. Holmgren, *Thioredoxin and related molecules-from biology to health and disease.* Antioxidants & redox signaling, 2007. **9**(1): p. 25-47.
168. Arnér, E.S. and A. Holmgren, *Physiological functions of thioredoxin and thioredoxin reductase.* European Journal of Biochemistry, 2000. **267**(20): p. 6102-6109.
169. Nordberg, J. and E.S. Arner, *Reactive oxygen species, antioxidants, and the mammalian thioredoxin system.* Free radical biology and medicine, 2001. **31**(11): p. 1287-1312.
170. Soerensen, J., et al., *The role of thioredoxin reductases in brain development.* PLoS One, 2008. **3**(3): p. e1813.
171. Young, J.J., A. Patel, and P. Rai, *Suppression of thioredoxin-1 induces premature senescence in normal human fibroblasts.* Biochemical and Biophysical Research Communications, 2010. **392**(3): p. 363-368.

172. Sharpless, N.E., *Ink4a/Arf links senescence and aging.* Experimental Gerontology, 2004. **39**(11–12): p. 1751-1759.
173. Guertin, D.A., et al., *Ablation in mice of the mTORC components raptor, rictor, or mLST8 reveals that mTORC2 is required for signaling to Akt-FOXO and PKCalpha, but not S6K1.* Dev Cell, 2006. **11**(6): p. 859-71.
174. Caccamo, A., et al., *Molecular interplay between mammalian target of rapamycin (mTOR), amyloid-beta, and Tau: effects on cognitive impairments.* J Biol Chem, 2010. **285**(17): p. 13107-20.
175. Xue, X., et al., *Single-Walled Carbon Nanotubes Alleviate Autophagic/Lysosomal Defects in Primary Glia from a Mouse Model of Alzheimer's Disease.* Nano Letters, 2014. **14**(9): p. 5110-5117.
176. Ohji, G., et al., *Suppression of the mTOR-raptor signaling pathway by the inhibitor of heat shock protein 90 geldanamycin.* J Biochem, 2006. **139**(1): p. 129-35.
177. Oshiro, N., et al., *Dissociation of raptor from mTOR is a mechanism of rapamycin-induced inhibition of mTOR function.* Genes Cells, 2004. **9**(4): p. 359-66.
178. Inoue, H., et al., *N-Formyl-3,4-methylenedioxy-benzylidene-gamma-butyrolaetam, KNK437 induces caspase-3 activation through inhibition of mTORC1 activity in Cos-1 cells.* Biochem Biophys Res Commun, 2010. **395**(1): p. 56-60.
179. Wang, X., et al., *The C terminus of initiation factor 4E-binding protein 1 contains multiple regulatory features that influence its function and phosphorylation.* Mol Cell Biol, 2003. **23**(5): p. 1546-57.
180. Fadden, P., T.A. Haystead, and J.C. Lawrence, Jr., *Identification of phosphorylation sites in the translational regulator, PHAS-I, that are controlled by insulin and rapamycin in rat adipocytes.* J Biol Chem, 1997. **272**(15): p. 10240-7.
181. Gingras, A.C., et al., *Hierarchical phosphorylation of the translation inhibitor 4E-BP1.* Genes Dev, 2001. **15**(21): p. 2852-64.
182. Raught, B., A.-C. Gingras, and N. Sonenberg, *6 Regulation of Ribosomal Recruitment in Eukaryotes.* Cold Spring Harbor Monograph Archive, 2000. **39**: p. 245-293.
183. Darzynkiewicz, Z., et al., *In search of antiaging modalities: evaluation of mTOR- and ROS/DNA damage-signaling by cytometry.* Cytometry A, 2014. **85**(5): p. 386-99.
184. Passos, J.F. and T. Zglinicki, *Mitochondrial dysfunction and cell senescence--skin deep into mammalian aging.* Aging (Albany NY), 2012. **4**(2): p. 74-5.
185. Essick, E.E. and F. Sam, *Oxidative stress and autophagy in cardiac disease, neurological disorders, aging and cancer.* Oxid Med Cell Longev, 2010. **3**(3): p. 168-77.
186. Scott, R.C., O. Schuldiner, and T.P. Neufeld, *Role and regulation of starvation-induced autophagy in the Drosophila fat body.* Dev Cell, 2004. **7**(2): p. 167-178.
187. Ravikumar, B., et al., *Inhibition of mTOR induces autophagy and reduces toxicity of polyglutamine expansions in fly and mouse models of Huntington disease.* Nature genetics, 2004. **36**(6): p. 585-595.
188. Rubinsztein, David C., G. Mariño, and G. Kroemer, *Autophagy and Aging.* Cell, 2011. **146**(5): p. 682-695.
189. Kenyon, C.J., *The genetics of ageing.* Nature, 2010. **464**(7288): p. 504-512.
190. Bjedov, I., et al., *Mechanisms of life span extension by rapamycin in the fruit fly Drosophila melanogaster.* Cell Metab, 2010. **11**(1): p. 35-46.

191. Selman, C., et al., *Ribosomal protein S6 kinase 1 signaling regulates mammalian life span.* Science, 2009. **326**(5949): p. 140-4.

APPENDIX A

SUPPLEMENTAL DATA

Table 1. Particle Size and Zeta Potential of TGA.

C_{70}-TGA	Z-ave (nm)	Polydispersity Index (PDI)	Z-potential (mv)
Experiment 1	119.7	0.382	-26.6
Experiment 2	111.8	0.282	-25.9
Experiment 3	110.4	0.355	-29.6
Average	111.2 ± 0.72	0.318 ± 0.05	-27.36 ± 1.95

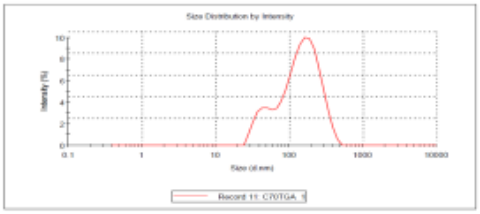

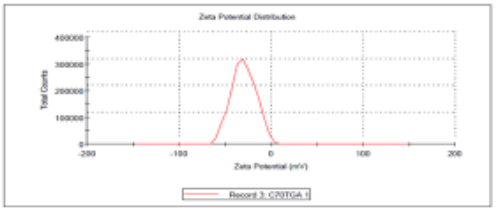

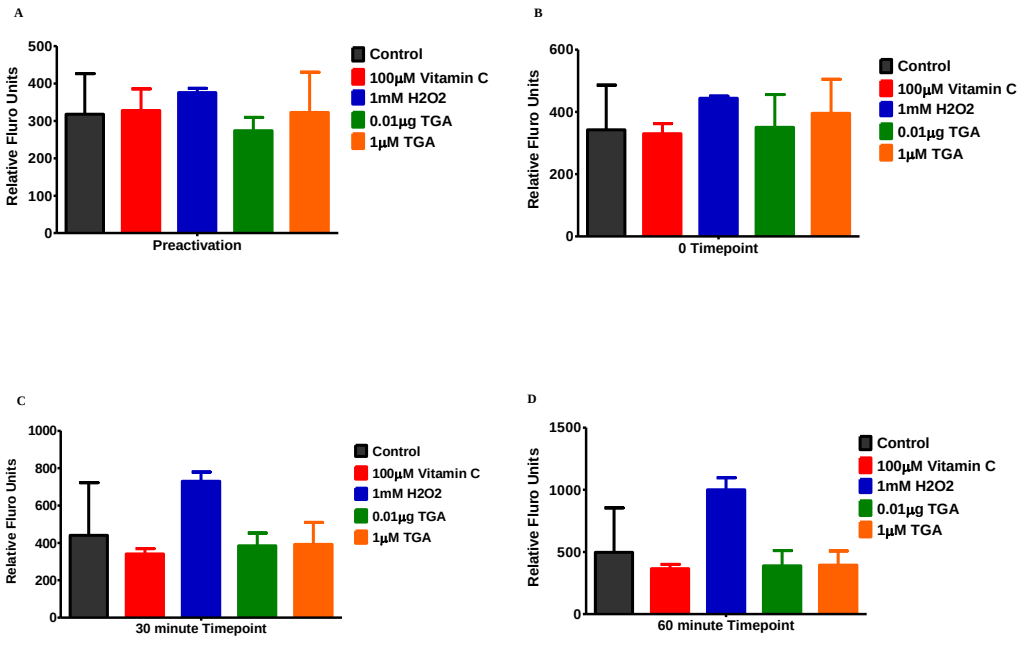

Figure 28. Relative Intensity of ROS generation using DCF assay. DCF analysis of intracellular generation of free radicals in response to C_{70}-TGA. ROS generation was not seen a

0.01 or1 µg TGA for all timepoints measured when compared to control. No significance was seen acrossall treamment groups. Experiment was conducted in triplicate and mean ± SD represented in graph.

Table 2. List of Proteins affected by TGA and/or 50 µM H_2O_2.

Target Protein	Phospho-site	%CFC 50µM H_2O_2	%CFC 1µg/ml TGA	%CFC 50µM H_2O_2/1µg/ml TGA
MEK2 mouse	T394	-30.70	-55.00	-66.23
IRS1	Y1179	-61.27	-33.90	-59.93
IR	Y972	-21.85	-7.93	-53.38
p38d MAPK	Y182	-9.99	-7.84	-52.65
ACTA1 (Alpha - actin)	Pan-specific	-35.31	-16.02	-52.01
p53	S392	-25.14	-5.04	-51.25
MEK2 human	T394	-34.93	-3.06	-50.71
p53	Pan-specific	-10.59	2.05	-50.69
MEKK1	Pan-specific	-37.88	-38.02	-50.14
Akt1 (PKBa)	Y474	-32.09	-11.64	-47.40
S6K	T412	-32.62	-22.07	-47.30
4E-BP1	S65	-45.84	-22.00	-47.03
p38b MAPK	T180+pY182	-16.28	-16.24	-46.36
p70 S6K	Pan-specific	-24.63	-12.09	-45.52
MEK1	S298	-41.64	-37.63	-44.65
PRAS40	T246	-17.87	-23.68	-44.43
MEK4	S257/T261	-9.47	-11.15	-41.18
MEK2	T394	-26.89	-7.64	-40.53
STAT3	Y704	-14.53	-15.08	-39.93
Abl	Y393	-24.16	-19.31	-39.09
MEK7	Pan-specific	-24.65	7.50	-38.51
Abl	Pan-specific	-8.50	-6.58	-37.68
MEK3b	Pan-specific	-10.44	-20.88	-35.90
MEK1	S292	-36.91	-8.61	-33.57
MKK3	S218	-3.10	-12.05	-33.17
JNK3	Pan-specific	-10.61	-12.64	-33.04
STAT5A	S780	-30.11	-5.19	-32.45
p70 S6K	S411	-15.98	4.78	-32.30
PTEN	S380/S382/S385	-33.53	-27.63	-31.80
MKK3	S189	-28.06	-3.47	-31.31
Vimentin	S33	-32.43	-10.49	-30.99

p70 S6K	T421/S424	-38.63	-5.19	-30.07
ATF2	T69+T71	-32.26	-20.55	-29.43
S6	S235	-38.23	-17.96	-27.70
Fos	T232	-14.74	9.54	-27.35
IKKa	Pan-specific	-0.65	-18.46	-26.21

*List of C_{70}-TGA and/or 50 μM H_2O_2 affected antibody microarray results (duplicate spots).
Site of phosphorylation is given after protein name. %CFC, percent change from control.

Table 2. List of Proteins affected by TGA and/or 50 µM H2O2. (Cont'd)

Target Protein	Phospho-site	%CFC 50µM H_2O_2	%CFC 1µg/ml TGA	%CFC 50µM H_2O_2/1µg/ml TGA
ASK1	S966	-17.00	-31.33	-25.33
IKKa	T23	0.34	1.01	-23.53
ERK1/2	T202+T185	-29.78	-19.22	-23.42
p70 S6K	S424	-10.76	35.21	-23.39
Jun	S73	-29.92	-17.29	-23.35
CDK1	Y19	-13.50	-4.97	-21.65
Hsc70	Pan-specific	-23.52	52.54	-21.30
MAPKAPK2	Pan-specific	-42.32	-18.68	-21.14
MEK3/6	S189 + S207	-34.36	-14.07	-20.20
SOD (Cu/Zn)	Pan-specific	-21.14	0.47	-19.93
DUSP10	Pan-specific	5.89	-7.12	-19.42
Cyclin D1	Pan-specific	22.37	3.43	-18.28
Akt1 (PKBa)	S473	-16.52	1.26	-18.16
p53	S6	-4.50	18.48	-16.95
Jun	Pan-specific	-24.50	-13.51	-16.37
eIF4G	S1108	-22.39	1.40	-16.20
p38a (MAPK 14)	Pan-specific	-12.19	12.90	-15.86
Shc1	Y239/Y240	6.63	-9.26	-15.53
STAT1	Y701	-14.81	3.39	-15.52
ERK1	Y204	-7.10	4.25	-15.33
Lyn	Pan-specific	-16.86	-0.77	-15.15
IRS1	Y612	-17.52	-22.33	-14.99
Hsp70	Pan-specific	-23.91	5.08	-14.86
MEK6	Pan-specific	-31.93	-8.54	-14.51
STAT1	S727	-1.51	-19.60	-14.21
p38a MAPK	Pan-specific	-2.15	-6.88	-13.89
DUSP11	Pan-specific	3.57	-4.23	-13.85
p53	S37	-3.75	18.78	-13.46
MEK1	T292	-25.19	-12.15	-13.31
Akt1 (PKBa)	Y326	-13.01	8.74	-12.91
MEK1	T386	1.69	18.28	-12.52
MEKK-NT	Pan-specific	19.08	-22.53	-12.46
Akt2 (PKBb)	Pan-specific	-7.32	-8.24	-10.41
DUSP12	Pan-specific	24.61	0.41	-10.34
Grp75	Pan-specific	8.49	23.62	-10.32
CDC42	Pan-specific	8.39	-16.64	-9.50
NFKB p65	S536	-17.17	-9.00	-8.91
MAPKAPK2	T334	-5.47	1.76	-8.84
eIF4E	S209	-26.33	-8.69	-8.30
IRS1	S639	25.76	-7.85	-7.58
VEGFR2	Y1214	-17.76	1.94	-7.49

*List of C_{70}-TGA and/or 50 µM H_2O_2 affected antibody microarray results (duplicate spots).
Site of phosphorylation is given after protein name. %CFC, percent change from control.

Table 2. List of Proteins affected by TGA and/or 50 µM H_2O_2. (Cont'd)

Target Protein	Phospho-site	%CFC 50µM H_2O_2	%CFC 1µg/ml TGA	%CFC 50µM H_2O_2/1µg/ml TGA
STAT5	Y694	5.89	-3.48	-7.39
ERK1/2	Pan-specific	-1.38	15.75	-7.23
Shc1	Y349	7.31	-12.87	-7.12
Grp78	Pan-specific	-15.23	2.51	-6.98
CDC7	T376	10.57	-9.35	-6.95
p38b MAPK	Pan-specific	17.02	4.14	-6.92
Hsp27	S15	-13.24	1.70	-6.58
DUSP2	Pan-specific	0.10	5.41	-6.38
p38g MAPK	Pan-specific	9.12	10.65	-6.33
ERK1/2	Y204+Y187	-13.39	13.87	-6.20
MAPKAPK5	T186	-13.15	1.10	-5.75
p38d MAPK	Pan-specific	10.32	-3.14	-5.48
Tubulin	Pan-specific	-23.20	-13.86	-2.97
PTEN	Pan-specific	0.69	-10.11	-2.19
p38a MAPK	T180+pY182	2.08	-4.54	-2.03
ERK5	Y221	-15.95	2.57	-1.07
PTEN	S380/T382/T383	5.12	11.06	-0.63
MELK	Pan-specific	21.32	-7.25	-0.47

*List of C_{70}-TGA and/or 50 µM H_2O_2 affected antibody microarray results (duplicate spots).
Site of phosphorylation is given after protein name. %CFC, percent change from control.

Table 2. List of Proteins affected by TGA and/or 50 µM H_2O_2. (Cont'd)

Target Protein	Phospho-site	%CFC 50µM H_2O_2	%CFC 1µg/ml TGA	%CFC 50µM H_2O_2/1µg/ml TGA
MKP2	Pan-specific	-14.65	-8.47	-0.26
A-Raf	Y302	2.26	-1.66	0.52
ERK1	T202+Y204	-19.55	-0.63	1.40
mTOR	S2448	26.83	-2.57	1.64
Hsp27	S78	-12.97	6.30	1.92
4E-BP1	Pan-specific	-8.86	-8.65	2.28
eIF4B	S422	-8.33	3.82	2.35
IRS1	S312	9.82	-10.69	2.42
Jun	Y170	-18.80	22.47	2.50
eIF4E	Pan-specific	-16.50	-24.60	3.08
MEK4	Pan-specific	-3.47	16.26	3.25
ERK4	S186	7.79	-10.52	3.34
MEK2	Pan-specific	13.54	37.62	3.45
ERK1	Y204+T207	12.39	37.78	4.19
Akt1 (PKBa)	Pan-specific	5.49	-8.91	4.44
DUSP5	Pan-specific	-4.35	1.25	4.98
STAT6	Pan-specific	-20.18	56.85	5.31
NFKB p65	S529	-1.47	13.79	6.20
4E-BP1	T45	-37.41	-0.54	6.53
JNK 1/2/3	T183/Y185	17.77	-1.93	6.54
GADD 153 (CHOP)	Pan-specific	45.40	6.15	6.60
Hsp27	S86	-6.56	2.20	7.22
ERK5	Pan-specific	-9.92	0.17	7.24
GroEL	Pan-specific	-3.44	-5.42	7.83
ALK	Y1507	37.88	30.23	8.92
MEKK2	Pan-specific	9.41	0.02	8.93
PI3-Kinase	Pan-specific	-28.91	-6.15	9.49
MEK1 + B23(NPM)	S217+S221	-9.03	60.75	9.54
STAT5A	Pan-specific	-22.59	-9.74	10.18
AMPKa2	S377	21.79	2.54	10.93
DUSP3	Pan-specific	35.71	20.45	11.25
VGFR1	Pan-specific	8.71	4.65	11.40
MDM2	S166	-11.96	6.06	11.70
MEK3/6	S189/193/S207/211	18.28	8.63	12.06

p21 CDKI1	Pan-specific	-8.01	25.47	12.30
VEGFR2	Y1059	-7.29	15.67	12.96

*List of C_{70}-TGA and/or 50 μM H_2O_2 affected antibody microarray results (duplicate spots).
Site of phosphorylation is given after protein name. %CFC, percent change from control.

Table 2. List of Proteins affected by TGA and/or 50 μM H_2O_2. (Cont'd)

Target Protein	Phospho-site	%CFC 50μM H_2O_2	%CFC 1μg/ml TGA	%CFC 50μM H_2O_2/1 μg/ml TGA
Insulin Receptor b	Pan-specific	-11.86	2.82	13.23
p38a MAPK	T180/Y182	-20.13	-7.00	13.53
MKK7	Pan-specific	-10.39	66.43	13.80
DUSP7	Pan-specific	27.15	-6.63	13.84
DUSP1 (MKP1)	Pan-specific	18.33	-2.90	13.89
JNK2	Pan-specific	-11.49	-9.01	13.91
NFKB p65 (Rel A)	S276	-12.14	-8.01	15.27
ERK1	S74	-5.29	13.82	15.95
MEK3	Pan-specific	21.91	88.77	16.50
MAPKAPK2	T222	-7.60	22.01	16.62
MKK3	Pan-specific	1.82	-7.73	16.76
ERK5	T219+Y221	0.42	13.40	17.29
MEK1	Pan-specific	2.91	6.35	17.71
STAT2	Y689	-12.12	4.87	17.72
Jun	S243	11.96	0.91	17.73
MEK5	Pan-specific	27.10	-6.63	18.12
ERK2	Pan-specific	11.59	9.82	18.18
CDK1	Pan-specific	9.70	-3.42	18.71
p70 S6K	T229	6.35	17.92	19.13
eIF2a	S52	1.57	3.24	19.62
STAT5B	Pan-specific	10.19	1.49	20.73
A-Raf	Pan-specific	28.82	8.36	22.08
p27 Kip1	Pan-specific	13.58	64.07	23.06
VGFR3	Pan-specific	-2.33	16.83	23.93
ERK5	T218+Y220	-4.01	20.48	25.31
NFkappaB p50	Pan-specific	-12.50	-0.64	25.84
DUSP9	Pan-specific	24.46	6.00	27.41
VEGF-C	Pan-specific	7.71	10.18	27.45
CREB1	S133	24.96	4.94	27.54
DUSP6	Pan-specific	13.61	1.02	27.83
NFkappaB p65	Pan-specific	-3.43	17.28	29.72
ERK1	T207	21.19	31.45	30.62
ERK1	Pan-specific	14.95	18.67	30.84
MKK6	Pan-specific	15.97	4.61	32.28
STAT1	Pan-specific	-4.96	43.28	34.17
STAT3	Pan-specific	-16.95	7.78	34.59

ERK3	Pan-specific	3.51	10.60	36.26
MKK3	Y230	-0.64	-14.56	37.98
Wee1	Pan-specific	33.47	57.59	40.52
Hsp105	Pan-specific	30.73	81.93	41.13
DUSP4	Pan-specific	28.29	7.31	41.20

*List of C_{70}-TGA and/or 50 μM H_2O_2 affected antibody microarray results (duplicate spots).
Site of phosphorylation is given after protein name. %CFC, percent change from control.

Table 2. List of Proteins affected by TGA and/or 50 μM H_2O_2. (Cont'd)

Target Protein	Phospho-site	%CFC 50μM H_2O_2	%CFC 1μg/ml TGA	%CFC 50μM H_2O_2/1μg/ml TGA
Jun	T91	14.50	20.12	42.22
MKK4	Pan-specific	25.57	8.86	42.99
mTOR	Pan-specific	29.19	9.25	43.74
eIF4G	S1232	11.01	43.61	44.99
eIF2a	Pan-specific	-0.12	21.32	46.50
DUSP8	Pan-specific	48.35	14.62	48.36
SODD	Pan-specific	57.80	14.61	49.15
ASK1	Pan-specific	31.91	21.90	49.63
CREB1	S129/S133	-2.39	23.31	53.17
JNK1	Pan-specific	49.99	-13.17	58.46
p53	S33	44.56	7.53	61.82
Fos	Pan-specific	76.56	25.02	64.69
STAT2	Pan-specific	71.08	57.53	65.77
VGFR2	Pan-specific	51.76	11.58	69.88
STAT4	Pan-specific	17.82	40.31	79.30
ATF2	S94/S112	-4.99	75.33	86.27
Grp94	Pan-specific	115.25	9.84	119.65

*List of C_{70}-TGA and/or 50 μM H_2O_2 affected antibody microarray results (duplicate spots).
Site of phosphorylation is given after protein name. %CFC, percent change from control.